Ocean Alkalinity Enhancement - Avoiding runaway CaCO$_3$ precipitation during quick and hydrated lime dissolution

5   Charly A. Moras[1,*], Lennart T. Bach[2], Tyler Cyronak[3], Renaud Joannes-Boyau[1], Kai G. Schulz[1]

[1]Faculty of Science and Engineering, Southern Cross University, Lismore, NSW, Australia
[2]Institute for Marine and Antarctic Studies, Ecology & Biodiversity, University of Tasmania, Hobart, TAS, Australia
[3]Department of Marine and Environmental Sciences, Nova Southeastern University, Fort Lauderdale, FL, USA

* *Correspondence to:* Charly A. Moras (c.moras.10@student.scu.edu.au)

10

Abstract. Ocean alkalinity enhancement (OAE) is a method that can remove carbon dioxide (CO$_2$) from the atmosphere and counteract ocean acidification, through the dissolution of alkaline minerals. Currently, critical knowledge gaps exist regarding the dissolution of different minerals suitable for OAE in natural seawater. Of particular importance, is to understand how much alkaline mineral can be dissolved before secondary precipitation of calcium carbonate (CaCO$_3$) occurs, since secondary CaCO$_3$
15   precipitation reduces the atmospheric CO$_2$ uptake potential of OAE. Using two types of minerals proposed for OAE, quick lime (CaO) and hydrated lime (Ca(OH)$_2$), we show that both (<63 µm of diameter) dissolved in seawater within a few hours. No CaCO$_3$ precipitation occurred at a saturation state (Ω_A) of ~5, but CaCO$_3$ precipitation in the form of aragonite occurred above an Ω_A value of 7. This limit is lower than expected for typical pseudo-homogeneous precipitation, i.e., in the presence of colloids and organic matter. Secondary precipitation at low Ω_A (~7) was the result of heterogeneous precipitation onto
20   mineral surfaces, most likely onto the added CaO and Ca(OH)$_2$ particles. Most importantly, runaway CaCO$_3$ precipitation was observed, a condition where significantly more total alkalinity (TA) was removed than initially added. Such runaway precipitation could reduce the OAE CO$_2$ uptake efficiency from ~0.8 moles of CO$_2$ per mole of added TA down to 0.1 mole of CO$_2$ per mole of TA. Runaway precipitation appears to be avoidable by dilution below the critical Ω_A threshold of 5, ideally within hours of the mineral additions to minimise initial CaCO$_3$ precipitation. Finally, OAE simulations suggest that for the
25   same Ω_A threshold, the amount of TA that can be added to seawater would be more than three times higher at 5 °C than at 30 °C. The maximum TA addition could also be increased by equilibrating the seawater to atmospheric CO$_2$ levels (i.e., to a pCO$_2$ of ~416 µatm) during addition. This would allow for more TA to be added in seawater without inducing CaCO$_3$ precipitation, using OAE at its CO$_2$ removal potential.

1 Introduction

Modern climate change is considered as one of the greatest threats to humankind (Hoegh-Guldberg et al., 2019; IPCC, 2021; The Royal Society and Royal Academy of Engineering, 2018). Global mean temperature has increased by 1.0 °C since pre-industrial times, and could reach +1.2-1.9 °C in the next 20 years, and +2.1-5.7 °C by the end of this century (IPCC, 2021). Furthermore, nearly 40% of anthropogenic carbon dioxide (CO_2) emissions have been taken up by the ocean through air-sea gas exchange between 1750 and 2020 (Friedlingstein et al., 2022). This has led to a decrease in the average open ocean pH by 0.1 unit in a process termed ocean acidification – OA (Bates et al., 2012; Canadell et al., 2007; Carter et al., 2019; Cyronak et al., 2014; Doney et al., 2009; Hoegh-Guldberg et al., 2007).

The CO_2 reduction pledged by the signatory states of the 2015 Paris Agreement aim to minimise the negative impacts of global warming and OA by limiting global warming to less than +2.0 °C, ideally below +1.5 °C, by the end of this century (Goodwin et al., 2018). However, the current and pledged reductions will likely not be enough and additional CO_2 mitigation strategies are needed, such as ocean alkalinity enhancement – OAE (Boyd et al., 2019; Gattuso et al., 2015; Lenton and Vaughan, 2009; The Royal Society and Royal Academy of Engineering, 2018). OAE could be an efficient approach for CO_2 removal (current emissions of 40 Gt per year), with models suggesting a potential of 165 to 790 Gigatonnes (1 Gt = 10^{15} g) of atmospheric CO_2 removed by the year 2100 on a global scale if OAE was implemented today (Burt et al., 2021; Feng et al., 2017; IPCC, 2021; Keller et al., 2014; Köhler et al., 2013; Lenton et al., 2018). However, empirical data on OAE efficacies is limited, and safe thresholds for mineral dissolution are particularly lacking (National Academies of Sciences and Medicine, 2021).

OAE typically relies on the dissolution of alkaline minerals in seawater, releasing alkalinity similar to natural rock weathering processes (Kheshgi, 1995). Suitable candidates are magnesium-rich minerals such as brucite, periclase or forsterite, and calcium-rich minerals such as quick and hydrated lime (Renforth and Henderson, 2017). Quick and hydrated lime are of particular interest, due to their high solubility in seawater and rapid dissolution. Quick lime, i.e., calcium oxide (CaO), is obtained by the calcination of limestone, composed primarily of calcium carbonate ($CaCO_3$), which is present in large quantities within the earth's crust. Once heated to temperatures of ~1200 °C, each molecule of $CaCO_3$ breaks down into one molecule of CaO and one molecule of CO_2 (Ilyina et al., 2013; Kheshgi, 1995). Hence, for maximum OAE potential, carbon capture during calcination and subsequent storage would be necessary (Bach et al., 2019; Ilyina et al., 2013; Kheshgi, 1995; Renforth et al., 2013; Renforth and Kruger, 2013). CaO can be hydrated into calcium hydroxide ($Ca(OH)_2$), also known as hydrated lime. The addition of either CaO or $Ca(OH)_2$ to seawater leads to the dissociation of $Ca(OH)_2$ into one calcium Ca^{2+} and two hydroxyl ions OH^- (Feng et al., 2017; Harvey, 2008). Ignoring the non-linearities of the seawater carbonate system (i.e., changes in total alkalinity, TA, and dissolved inorganic carbon, DIC, are not 1:1), the chemical reaction of CO_2 and $Ca(OH)_2$ dissolution and the subsequent uptake of atmospheric CO_2 can be written as:

$$(CaO + H_2O \rightleftharpoons Ca(OH)_2) + 2CO_2 \rightarrow Ca^{2+} + 2HCO_3^- \qquad\qquad 1$$
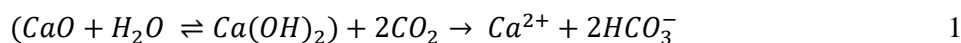
The dissolution of CaO and Ca(OH)$_2$ and the subsequent addition of TA increases the pH of seawater, which changes the carbonate chemistry speciation (Zeebe and Wolf-Gladrow, 2001). DIC can be approximated as the sum of HCO$_3^-$ and CO$_3^{2-}$ (ignoring the small contribution by CO$_2$). Similarly, TA can be approximated as the sum of HCO$_3^-$ and 2 CO$_3^{2-}$ (ignoring the smaller contributions by boric and silicic acid, and other minor components). Combining both DIC and TA equations reveal that CO$_3^{2-}$ concentrations can be expressed as [CO$_3^{2-}$] = TA-DIC. Hence, increasing TA at a constant DIC, e.g., by dissolving CaO or Ca(OH)$_2$, increases [CO$_3^{2-}$], shifting the carbonate chemistry speciation towards a higher pH (Figure A1) (Dickson et al., 2007; Wolf-Gladrow et al., 2007; Zeebe and Wolf-Gladrow, 2001). The subsequent shift in DIC speciation leads to a decrease in dissolved CO$_2$ concentrations, reducing the partial pressure of CO$_2$ (pCO$_2$) in seawater and increasing its atmospheric CO$_2$ uptake potential.

Depending on the amount of TA added and the initial seawater pCO$_2$, the TA-enriched seawater would either take up CO$_2$ from the atmosphere or reduce outgassing of CO$_2$. Factoring in the non-linearities of the carbonate system, about 1.6 moles of atmospheric CO$_2$ could be taken up per mole of dissolved CaO or Ca(OH)$_2$ (Köhler et al., 2010). Furthermore, dissolving CaO and Ca(OH)$_2$ can also counteract ocean acidification. During the dissolution of alkaline minerals, both pH and the CaCO$_3$ saturation state of seawater (Ω) increase through increasing Ca^{2+} and CO$_3^{2-}$ concentrations. This makes OAE a dual solution for removing atmospheric CO$_2$ and mitigating OA (Boyd et al., 2019; Feng et al., 2017; Harvey, 2008). However, there are important knowledge gaps in our understanding surrounding basic mineral dissolution in seawater (Feng et al., 2016; González and Ilyina, 2016; Mongin et al., 2021; Renforth and Henderson, 2017).

One knowledge gap is the critical Ω threshold beyond which CaCO$_3$ starts to precipitate inorganically. Such secondary precipitation constitutes the opposite of alkaline mineral dissolution and would decrease pH and Ω, while simultaneously increasing the CO$_2$ concentration in seawater. This would decrease the ocean uptake's capacity for atmospheric CO$_2$, having the opposite of the intended effect. Additionally, if all added alkalinity is precipitated, only one mole of atmospheric CO$_2$ per mole of Ca^{2+} would be removed, instead of ~1.6 in the absence of CaCO$_3$ precipitation. If even more CaCO$_3$ precipitates, the efficiency of OAE would be further reduced. At typical seawater conditions, CaCO$_3$ precipitation does not occur due to the absence of mineral phase precipitation nuclei and the presence of precipitation inhibitors such as dissolved organic compounds, magnesium (Mg) or phosphate (Chave and Suess, 1970; De Choudens-Sanchez and Gonzalez, 2009; Pytkowicz, 1965; Rushdi et al., 1992; Simkiss, 1964). There are three types of CaCO$_3$ precipitation, 1) homogeneous (in the absence of any precipitation nuclei), 2) heterogeneous (in the presence of mineral phases), and 3) pseudo-homogeneous (in the presence of colloids and organic materials) (Marion et al., 2009; Morse and He, 1993). For pseudo-homogeneous precipitation, the critical threshold at which calcite precipitates spontaneously is at a calcite saturation state (Ω_C) of ~18.8 (at a salinity of 35 and at a temperature of 21 °C) (Marion et al., 2009). Assuming typical open-ocean carbonate chemistries (e.g., TA ~2350 µmol kg^{-1} and DIC ~2100 µmol kg^{-1}), this threshold would be reached through an increase in TA of ~810 µmol kg^{-1}. This corresponds to a critical threshold for Ω with respect to aragonite, i.e., Ω_A, of ~12.3. The two other types of precipitation (i.e., homogeneous and

3

heterogeneous), are more poorly constrained (Marion et al., 2009). Importantly, at current dissolved Mg and Ca concentrations in seawater, the CaCO$_3$ polymorph that is favoured during inorganic precipitation is aragonite rather than calcite (Morse et al., 1997; Pan et al., 2021). Therefore, aragonite saturation state Ω_A may be a more important determinant of critical runaway precipitation thresholds. No matter what mineral phase is precipitating, a better understanding of CaCO$_3$ precipitation under conditions relevant to OAE are needed.

To gain a better understanding on the consequences of CaO and Ca(OH)$_2$ dissolution for OAE, we conducted several dissolution experiments with CaO and Ca(OH)$_2$ to determine 1) how much alkaline material can be dissolved without inducing CaCO$_3$ precipitation, 2) what causes secondary CaCO$_3$ precipitation, and 3) how secondary precipitation can be avoided.

2 Material & Methods

2.1 Experimental setup

Two different calcium minerals were used, CaO powder from Ajax Finechem (CAS no 1305-78-8) and industrial Ca(OH)$_2$ powder (Hydrated Lime 20kg, Dingo). The elemental compositions of these powders were analysed using an Agilent 7700 Inductively Coupled Plasma Mass Spectrometer, coupled to a laser ablation unit (NWR213, Electro Scientific Industries, Inc). Samples were embedded in resin and instrument readings calibrated against standard reference materials, batches #610 and #612, from the National Institute of Standards and Technology.

All dissolution experiments were conducted in natural seawater. The seawater was collected between September 2020 and June 2021, about 200 to 300 m from the shore, avoiding suspended sand or silt, at Broken Head, New South Wales, Australia (28°42'12" S, 153°37'03" E). Seawater was stored up to 14 days at 4 °C in the dark to slow bacterial metabolic activity and allow for all suspended particles to settle on the bottom before being sterile-filtered using a peristaltic pump, connected to a 0.2 µm Whatman Polycap 75 AS filter. For salinity measurements, about 200 mL of seawater were placed in a gas-tight polycarbonate container and allowed to equilibrate to room temperature overnight. The sample's conductivity and temperature were then measured with a Metrohm cell (6.017.080), connected to a 914 pH/Conductometer. The conductivity was recorded in millisiemens per cm (mS/cm), and the temperature in °C. Salinity was calculated according to Lewis and Perkin (1981) on the 1978 practical salinity scale. The salinity in each experiment is reported in Table A1.

2.2 OAE experiments

For each experiment, seawater was accurately weighed (in grams to 2 decimal places) into high-quality borosilicate 3.3 2 L Schott Duran beakers, and the temperature was controlled via a Tank Chiller Line TK 1000 set at 21 °C, feeding a re-circulation water jacket (Figure A2). A magnetic stir bar was placed in the beaker, and the natural seawater was constantly stirred at ~200 rpm. To minimise gas exchange, a floating lid with various sampling ports was placed on top. Finally, after one hour of equilibration, calculated amounts of weighed-in calcium alkaline compounds were added. Upon addition, samples for DIC and TA were taken at increasing time intervals to fully capture the dissolution kinetics and check for potential secondary

4

precipitation. Furthermore, the pH was monitored at a frequency of 1 Hertz for the first hour before alkalinity addition, and over 4 hours after addition to determine when alkalinity was fully released. Once the pH plateaued (corresponding to maximum TA release), the content of the beaker was carefully transferred to a clean Schott bottle to ensure that evaporation would not alter the DIC or TA concentrations. Bottles were kept in the dark for the duration of each experiment, i.e., up to 48 days, with the same constant stirring of ~200 rpm at 21 °C. Each bottle was exposed to UV light for at least 30 minutes after each sampling to inhibit bacterial growth.

2.2.1 CaO and Ca(OH)$_2$ dissolution

Following the beaker setup as described in section 2.2, TA was added by sieving CaO and Ca(OH)$_2$ through a 63 µm mesh, to avoid the formation of larger CaO or Ca(OH)$_2$ aggregates. The mesh was placed in a clean upside-down 50 mL Falcon tube cap, to minimise the loss of material smaller than 63 µm, and the overall weight was recorded in mg. Then, the mesh was placed above the Schott bottle, and mineral was added by gently tapping the side of the sieve. Finally, the sieve was placed in the same upside-down Falcon tube cap and weighed once again, thereby making sure that the desired amount had been added to the beaker. The weighing steps were carefully performed to avoid material loss between the bottle and the balance, and were achieved in less than five minutes. Two alkalinity additions, +250 and +500 µmol kg^{-1} with each calcium mineral powder were performed (Table 1).

2.2.2 Na$_2$CO$_3$ alkalinity, particles additions, and filtration

Three further experiments assessed the role of mineral phases during secondary CaCO$_3$ precipitation observed in the previous experiments. The first experiment used a 1M solution of sodium carbonate (Na$_2$CO$_3$, CAS number 497-19-8), freshly prepared on the day to limit CO$_2$ ingassing. Ultrapure Na$_2$CO$_3$ was accurately weighed (in mg with 2 decimal places), into a clean 100 mL Schott bottle and made up to 100 g with MilliQ (18.2 MΩ). The solution was then sonicated for 15 minutes, with gentle mixing every five minutes. The amount of Na$_2$CO$_3$ to be added to seawater was calculated so that a similar maximum Ω_A would be reached, i.e., ~7.7, as in the previous experiments with the highest addition of CaO and Ca(OH)$_2$. This required about twice the alkalinity increase as before (Table 1), because Na$_2$CO$_3$ additions concomitantly increase DIC when dissociating in two sodium and one CO$_3^{2-}$ ion, making the Ω_A increase smaller. All carbonate chemistry calculations were done in CO$_2$SYS (see below).

In another similar experiment to the Na$_2$CO$_3$ addition, quartz powder was added after two days. Quartz powder was chosen as it does not dissolve on the timescales relevant for this study (Montserrat et al., 2017). The addition of quartz powder was similar to the sieved CaO and Ca(OH)$_2$ additions, i.e., through a 63 µm mesh. The mass of quartz particles added (in mg with 2 decimal places), was determined to provide the same mineral surface area as for the Ca(OH)$_2$ experiments with a TA increase of 500 µmol kg^{-1}. It was calculated using densities and masses of Ca(OH)$_2$ and quartz, assuming spherical particles with a diameter of 63 µm.

The third experiment followed the same experimental setup as described in section 2.2.1. Here, Ca(OH)$_2$ was added to first increase TA by ~500 µmol kg^{-1} (Table 1). After 4 h of reaction, the entire content of the 2L Schott beaker was filtered through a Nylon Captiva Econofilter (25mm) with a pore size of 0.45 µm into a clean 1L Schott bottle using a peristaltic pump. The bottle was filled from bottom to top, with overflow to minimise gas exchange.

2.2.3 Dilution experiments

In a last set of experiments, alkalinity enriched seawater was diluted with natural seawater, to test if secondary precipitation can be avoided or stopped. Ca(OH)$_2$ powder was added to reach final alkalinity enrichments of 500 and 2000 µmol kg^{-1} and dilutions were carried out at several time intervals.

For the experiment with a targeted TA increase of 500 µmol kg^{-1}, a larger quantity of TA-enriched seawater was required to perform all dilutions and sampling in comparison to the previous experiments. Therefore, two 5L Schott bottles were filled with 5kg of natural seawater and placed on a magnetic stirring platform. Calculated weighed-in masses of Ca(OH)$_2$ were added to the first bottle, as described in section 2.2.1, using the 63 µm sieve, while the natural seawater in the second bottle was kept for subsequent dilutions. Both bottles were kept on the same bench under the same conditions, stirring at a rate of ~200 rpm, for the duration of the experiment.

Following the Ca(OH)$_2$ addition, 1:1 dilutions (500 g TA-enriched seawater:500 g natural seawater) were performed in clean 1L Schott bottles that were kept in the dark and placed on a magnetic platform at a stirring rate of ~200 rpm. After each sampling time, the bottles were exposed to UV light for at least 30 minutes. The second dilution experiment was set up like the first one, the only difference being that the targeted TA increase was 2000 µmol kg^{-1}. The dilution ratio was 1:7 to reduce the targeted TA increase again to 250 µmol kg^{-1}. All dilutions were performed 10 minutes, 1 hour, 1 day and 1 week after Ca(OH)$_2$ addition, leading to two TA-enriched and eight diluted treatments.

2.3 Carbonate chemistry measurements

Samples for TA and DIC measurements were filtered through a Nylon Captiva Econofilter (0.45 µm) using a peristaltic pump into 100 mL Borosilicate 3.3 Schott DURAN glass stopper bottles. The bottles were gently filled from the bottom to top, using a 14-gauge needle as described in Schulz et al. (2017), with at least half of their volume allowed to overflow, corresponding to ~150 mL of seawater sampled per time-point. After filling, 50µL of saturated mercuric chloride solution were added to each sample before being stored without headspace in the dark at 4 °C.

TA was analysed in duplicate via potentiometric titrations by a Metrohm 848 Titrino Plus coupled to an 869 Compact Sample Changer using 0.05M HCl, with the ionic strength adjusted to 0.72 mol kg^{-1} using NaCl, corresponding to a salinity of 35. Titrations and calculations followed the open-cell titration protocols by Dickson et al. (2007). DIC was measured in triplicate using an Automated Infra-Red Inorganic Carbon Analyzer (AIRICA, Marianda) coupled to a LICOR Li7000 Infra-Red detector as described in Gafar and Schulz (2018). Measured values of TA and DIC were corrected using an internal standard prepared as described in Dickson (2010), calibrated against Certified Reference Materials Batch #175 and #190.

190　　　　The overall instruments uncertainty for TA and DIC was calculated as follows. For each measurement, a standard deviation was calculated, from duplicates of TA and triplicates of DIC. The samples and reference materials standard deviations were averaged, and an error propagation on these values were used to estimate average measurement uncertainty, i.e., $\pm$ 1.0 µmol kg^{-1} and DIC at $\pm$ 0.8 µmol kg^{-1}, for TA and DIC, respectively.

2.4 Particulate Inorganic Carbon and Scanning Electron Microscopy (SEM)

195　　　　In cases where TA and DIC decreases were observed, indicative of $CaCO_3$ precipitation, samples were taken at the end of the experiments for total particulate carbon (TPC), particulate organic carbon (POC) and scanning electron microscopy (SEM) analyses. TPC and POC samples were collected in duplicates on pre-combusted (450 °C) GF/F filters and stored frozen until analysis. Before analysis, POC filters were fumed with HCl for 2 hours before drying over night at 60 °C while TPC filters were dried untreated (Gafar and Schulz, 2018). The filters were wrapped in tin capsules and pressed into small 5 mm

200　diameter balls. TPC and POC were quantified on a Thermo-Fisher Elemental Analyser Flash EA, coupled to a Delta V Plus Isotope Ratio Mass Spectrometer. Particulate inorganic carbon (PIC), or $CaCO_3$, was calculated based on the difference between TPC and POC. The results are reported in µmol kg^{-1} of seawater with an uncertainty estimate by an error propagation of the square root of the sum of the squared standard deviations for TPC and POC.

　　　　For SEM analysis, 10 to 15 mL of the sample water was collected on polycarbonate Whatman Cyclopore filters with

205　a 0.2 µm pore size and rinsed with 50 mL of MilliQ. The filters were dried at 60 °C overnight and kept in a desiccator until analysis on a tabletop Hitachi Scanning Electron Microscope TM4000 Plus. The microscope was coupled to an Energy Dispersive X-Ray (EDX) Analyser, allowing to identify the $CaCO_3$ polymorph and elemental composition of precipitates. Finally, CaO and $Ca(OH)_2$ powders were analysed for their carbon content. This analysis aimed to identify the presence and estimate the amount of particulate carbon, most likely $CaCO_3$, in the respective mineral powders.

210　**2.5 Carbonate chemistry calculations**

Measured DIC, TA, temperature and salinity were used to calculate the remaining carbonate chemistry parameters with the CO_2SYS script for MATLAB® (MathWorks). The borate to salinity relationship and boric acid dissociation constant from Uppstrom (1974), and the carbonic acid dissociation constants of Lueker et al. (2000) were used. With two measured carbonate chemistry parameters, i.e., DIC and TA, the others can be derived. An important difference in our experiments was that the

215　dissolution of CaO and $Ca(OH)_2$ changed the calcium concentration and hence the salinity-based Ω calculated by CO_2SYS is underestimated. Ω is defined by the solubility product of $CaCO_3$ as:

$$\Omega = \frac{[Ca^{2+}] \times [CO_3^{2-}]}{K_{sp}} \qquad\qquad 2$$

where [Ca^{2+}] and [CO$_3$$^{2-}$] denote seawater concentrations of Ca^{2+} and CO$_3$$^{2-}$, and K$_{sp}$ is the solubility product for calcite or aragonite at the appropriate salinity and temperature. To calculate saturation states, the correct calcium concentration [Ca^{2+}]$_{Corr}$ was estimated from measured salinity (Riley and Tongudai, 1967) and half the alkalinity concentration change, ΔTA, generated during CaO or Ca(OH)$_2$ dissolution or loss due to CaCO$_3$ precipitation:

$$[Ca^{2+}]_{Corr} = \frac{0.01028}{35} \times \text{Salinity} + \frac{\Delta TA}{2} \qquad \qquad 3$$

where 0.01028 is the molar Ca^{2+} concentration at a salinity of 35. K$_{sp}$ was calculated from in-situ temperature and salinity according to Mucci (1983). The correct Ω$_C$ and Ω$_A$ were then calculated according to Equation 2. Please note that we have opted to report Ω$_A$ rather than Ω$_C$ since aragonite is more likely to be precipitated in natural modern seawater (Morse et al., 1997).

2.6 OAE simulations

CO$_2$SYS and the results from the various dissolution experiments were used to simulate three OAE scenarios (Table 3). Three alkalinity additions were simulated, +250, +500 and +1000 µmol kg^{-1}. The starting parameters were TA = 2350 µmol kg^{-1}, DIC = 2100 µmol kg^{-1}, salinity = 35, temperature = 19 °C, using the same acid-base equilibrium constants as described in section 2.5. In the first scenario, for all three additions, no CaCO$_3$ precipitation was assumed. We then estimated the amount of CO$_2$ taken up by the seawater after atmospheric re-equilibration, i.e., until a pCO$_2$ of ~416 ppm. For the +500 and +1000 µmol kg^{-1} TA increases, two additional simulations were performed. First, we assumed that as much CaCO$_3$ precipitated as TA was added, e.g., after increasing the TA by 500 µmol kg^{-1}, we assumed a loss of 500 µmol kg^{-1} of TA and 250 µmol kg^{-1} of DIC. We then simulated atmospheric re-equilibration until a pCO$_2$ of ~416 ppm and recorded the changes in the carbonate chemistry parameters. Second, we assumed that CaCO$_3$ precipitated down to an Ω$_A$ of ~2 as observed in our experiments. After calculating full carbonate chemistry speciation in these various scenarios, the amount of CO$_2$ taken up after atmospheric re-equilibration was determined using the same approach as described above.

3 Results

3.1 Chemical composition of CaO and Ca(OH)$_2$

The bulk chemical composition of the CaO and Ca(OH)$_2$ powders were analysed. These consisted primarily of calcium, with minor contributions of magnesium and silicon (see Table A2, for a more comprehensive list). Furthermore, CaO and Ca(OH)$_2$ contained about 9.4 ±0.1 mg g^{-1} and 18.0 ±0.2 mg g^{-1} of particulate carbon respectively, i.e., ~0.9% and ~1.8% by weight.

3.2 CaO dissolution in filtered natural seawater

In the first CaO experiment with a targeted 250 µmol kg^{-1} TA addition, TA increased by ~200 µmol kg^{-1} within the first 4 hours (Figure 1a). Following this increase, TA was stable over time. In contrast, DIC increased slowly, about 1 µmol kg^{-1} per day, reaching about +50 µmol kg^{-1} on day 47 of the experiment (Figure 1b). Ω_A reflected the trend observed for ΔTA, increasing from ~2.9 to ~5.1 within the first 4 hours before slowly decreasing to 5.0 on day 47 (Figure 1c).

In the second CaO experiment with a targeted 500 µmol kg^{-1} TA addition, TA increased by ~410 µmol kg^{-1} within the first 4 hours before slowly decreasing on day 3 (Figure 1a). This was followed by a rapid decrease over the following week, eventually reaching a steady state on day 20 at a final ΔTA of about -540 µmol kg^{-1}. It corresponds to a total loss of TA of ~950 µmol kg^{-1}, between the maximum measured TA and the final recorded TA. A small decrease in DIC of ~10 µmol kg^{-1} was observed over the first two days before a more significant reduction in the following week. Finally, ΔDIC levelled off at about -465 µmol kg^{-1} (Figure 1b). Ω_A rapidly increased during the first 4 hours of the experiment from 2.8 up to 7.6 (Figure 1c). Following this quick increase, Ω_A decreased by 0.3 unit by day 3. Afterwards, Ω_A dropped quickly to 2.4 on day 13, and reached ~1.8 on day 47, corresponding to a reduction of 1.0 compared to the starting seawater value.

3.3 Ca(OH)$_2$ dissolution in filtered natural seawater

In the first Ca(OH)$_2$ experiment with a targeted TA addition of 250 µmol kg^{-1}, TA increased by ~220 µmol kg^{-1} after 4 h of reaction, before stabilising at a ΔTA of ~210 µmol kg^{-1} for the rest of the experiment (Figure 2a). The DIC concentration increased quickly over the first 6 days after the TA addition before slowing down, reaching about +70 µmol kg^{-1} by the end of the experiment (Figure 2b). Finally, Ω_A reached ~4.1 after 4 hours, slightly decreasing over time, reaching 3.3 on day 28 (Figure 2c).

In the second Ca(OH)$_2$ experiment with a targeted TA addition of 500 µmol kg^{-1}, TA increased by ~440 µmol kg^{-1} within the first 4 h (Figure 2a). This was followed by a steady decrease of ~18 µmol kg^{-1} per day over the next 2 weeks, after which the decrease accelerated to ~28 µmol kg^{-1} per day until day 35. Then, it levelled off at a ΔTA of about -420 µmol kg^{-1} towards the end of the experiment. Overall, ~860 µmol kg^{-1} of TA were lost compared to the highest TA recorded. The overall DIC concentration decreased in a similar fashion as TA, reaching a ΔDIC of about -395 µmol kg^{-1} compared to the initial DIC concentration (Figure 2b). Ω_A increased from 2.5 to 7.4 in the first 4 hours before decreasing, similarly to TA and DIC, reaching ~2.0 on day 42 (Figure 2c).

3.4 Na$_2$CO$_3$, particle addition and filtration

Three experiments assessed the influence of particles on CaCO$_3$ precipitation. In the first one, ~1050 µmol kg^{-1} of TA was added using a 1M Na$_2$CO$_3$ solution, designed to obtain a similar maximum Ω_A as the previous experiments when TA decreased (Table 1). Upon addition, TA increased by ~1060 µmol kg^{-1} and DIC by ~530 µmol kg^{-1} within minutes. For the remainder of the experiment, ΔTA was fairly constant between 1060 and 1040 µmol kg^{-1} (Figure 3a). In contrast, DIC slightly

increased over 42 days from a ΔDIC of ~530 µmol kg^{-1} on day 1 to ~560 µmol kg^{-1} on day 42 (Figure 3b). Ω_A increased from ~2.3 to ~8.5 within minutes of the Na_2CO_3 addition and slightly decreased to ~8.1 after 42 days of experiment (Figure 3c).

In the second experiment, the addition of 1M Na_2CO_3 solution (Table 1) increased TA by 1070 µmol kg^{-1}, while DIC increased by ~540 µmol kg^{-1} within minutes and remained stable (Figure 3a, 3b). After 2 days, quartz particles were added. Whereas ΔTA and ΔDIC remained invariant after one day, ΔTA decreased to ~220 µmol kg^{-1} and ΔDIC dropped to ~120 µmol kg^{-1} between day 5 and 12 (Figure 3a, 3b). Over the next month, ΔTA and ΔDIC continued to decrease, although at a slowing rate, reaching about -200 and -110 µmol kg^{-1}, respectively on day 42. Ω_A followed a similar trend, with an increase from ~2.8 up to ~9.2 within the first 1.5 hours, and a significant decline to ~3.9 between day 5 and day 12, before stabilizing around ~2.0 at the end of the experiment on day 48.

In the last experiment, $Ca(OH)_2$ was added, aiming for a TA increase of 500 µmol kg^{-1} (Table 1), a level at which a significant TA decrease had been observed previously (Figure 2a). In contrast to the previous experiment, after reaching ~470 µmol kg^{-1} at the 4-hour mark, the content of the bottle was filtered and ΔTA remained relatively constant between 465 and 470 µmol kg^{-1} over the following 48 days of experiment (Figure 3a). Meanwhile, ΔDIC increased from ~5 to 55 µmol kg^{-1} after filtration (Figure 3b). Ω_A increased from ~2.8 to ~8.2 within the first 1.5 hours after $Ca(OH)_2$ addition, and then slightly decreased to ~7.5 over the 48 days of experiment (Figure 3c).

3.5 Dilution experiments

3.5.1 500 µmol kg^{-1} addition

In these experiments with a targeted TA increase of 500 µmol kg^{-1} by $Ca(OH)_2$ addition, ΔTA increased to ~450 µmol kg^{-1} after 2 hours (Figure 4). These changes in TA were followed by a decline to ~320 µmol kg^{-1} after 14 days, although the latter was a slightly slower decrease than previously (Figure 2Figure 4a). After a first increase in ΔDIC by ~10 µmol kg^{-1} on day 1, ΔDIC steadily decreased to about -20 µmol kg^{-1} after two weeks (Figure 4b). Finally, Ω_A increased from ~2.7 to ~7.8 after 2 hours, before steadily decreasing to ~6.4 on day 14 (Figure 4c).

In the diluted treatments, ΔTA remained relatively stable over time, until the end of the experiments on day 29, regardless of dilution time (Figure 4a). Upon dilution, ΔTA was reduced, which were similar for the 10-minute, 1-hour and 1-day dilutions. Overall, in the 1-week dilution, ΔTA was slightly lower, i.e., ~205 µmol kg^{-1} instead of ~230 µmol kg^{-1} on average. In all dilutions, ΔDIC increased over time, ranging between ~20 µmol kg^{-1} and ~60 µmol kg^{-1}, independent of dilution timing. Finally, Ω_A showed similar trends to ΔTA, reaching between ~4.8 and ~5.2, and slightly decreasing over time until the end of the experiment.

3.5.2 2000 µmol kg^{-1} addition

This set of experiments aimed for a TA increase of 2000 µmol kg^{-1} by $Ca(OH)_2$ addition. However, TA only increased to ~⅓ of the targeted value, i.e., ~725 µmol kg^{-1} within the first two hours (Figure 4d). Following this increase, TA rapidly

decreased during the first day, reaching a ΔTA of about -1260 µmol kg^{-1}, and -1440 µmol kg^{-1} in the following week (Figure 4d). Over the second week of the experiment, TA appeared to stabilise before increasing until day 21. In contrast, ΔDIC decreased by ~580 µmol kg^{-1} within the first two hours, before rapidly dropping to about -1590 µmol kg^{-1} on day 1, and -1660 µmol kg^{-1} after 7 days (Figure 4e). Over the remaining 41 days, ΔDIC increased by ~210 µmol kg^{-1}, remaining ~1450 µmol kg^{-1} below the starting DIC concentration. Ω_A increased to ~16.7 after 2 hours, followed by a rapid drop to ~3.2 on day 1 and ~2.0 on day 14, while slightly increasing the following 34 days, varying between 2.0 and 2.1 (Figure 4f).

With respect to ΔTA, ΔDIC and Ω_A, the 10-minute and 1-hour dilutions showed similar responses, as did the 1-day and 1-week dilutions. Upon dilution, ΔTA reached values of ~240 µmol kg^{-1} after the 10-minute and 1-hour dilutions, and about -160 to -190 µmol kg^{-1} after the 1-day and 1-week dilutions. With the exception of one data point in the 1-week dilution data, ΔTA remained relatively constant throughout all dilution experiments (Figure 4d). DIC changes were similar to the TA changes, slowly increasing over time between 0.6 and 2.5 µmol kg^{-1} per day, with very similar values reached for the 10-minute and 1-hour dilutions, as opposed to the 1-day and 1-week dilutions (Figure 4e). Finally, Ω_A dropped from ~5.0-5.1 to ~4.0-4.1 over time in the 10-minute and 1-hour dilutions, while it decreased from ~2.3-2.8 to ~2.1-2.2 until day 21 in the 1-day and 1-week dilutions, before increasing to ~2.6-3.4 toward the end of the experiments (Figure 4f).

3.6 Particulate inorganic carbon

With the exception of the ~1050 TA addition by Na_2CO_3 and quartz particles, measured PIC in experiments was always higher than estimates from measured ΔTA (Table 2). Furthermore, PIC estimated from the theoretical maximum TA increase upon full mineral dissolution, ΔTA_{Theo}, was always higher than estimated PIC from ΔTA, by about 7 to 14% in the ~500 µmol kg^{-1} TA additions with $Ca(OH)_2$ and CaO, respectively, and up to 67% in the experiment with ~2000 µmol kg^{-1} TA additions.

4 Discussion

This study presents the first results investigating the dissolution of CaO and $Ca(OH)_2$ in natural seawater in the context of OAE. In experiments with at least 500 µmol kg^{-1} TA increase, secondary precipitation was detected through observed TA and DIC decreases, as well as PIC increases. More specifically, at TA additions leading to an Ω_A higher than 7 (in the +500 and +1000 µmol kg^{-1} TA treatments), "runaway $CaCO_3$ precipitation" was observed, meaning that not only the added TA was completely removed, but significant portions of residual seawater TA as well, until a new steady state was reached. This vastly reduces the desired CO_2 removal potential by OAE and should therefore be avoided. In a subsequent set of experiments, we simulated ocean mixing to estimate the timescales required to avoid and/or stop secondary $CaCO_3$ precipitation for applications that initially have TA additions above the critical threshold.

11

4.1 Identifying CaCO₃ precipitation, the problem of unmeasured precipitation, and CO₂ gas exchange

$CaCO_3$ precipitation can occur via three pathways, i.e., heterogeneous, homogeneous and pseudo-homogeneous nucleation and precipitation (Chen et al., 2005; Marion et al., 2009; Wolf et al., 2008). Heterogeneous precipitation relies on the presence of existing solid mineral surfaces. This differs from homogeneous precipitation, characterised by the formation of $CaCO_3$ crystals from Ca^{2+} and CO_3^{2-} ions in the absence of any nucleation surfaces (Chen et al., 2005; Wolf et al., 2008). Finally, the last type of precipitation, termed pseudo-homogeneous, is similar to homogeneous nucleation, but it occurs on nuclei other than solid minerals such as colloids, organic particles or glassware in a laboratory setting (Marion et al., 2009). Concerning the Ω thresholds above which $CaCO_3$ precipitation is expected, the lowest threshold would be for heterogeneous and the highest for homogeneous, with pseudo-homogeneous nucleation in between. This is because nucleation sites effectively lower the activation energy required for $CaCO_3$ precipitation (Morse et al., 2007).

When 1 mole of $CaCO_3$ is precipitated, the TA of the solution decreases by 2 moles due to the removal of 1 mole of CO_3^{2-} ions, accounting for 2 moles of TA (Zeebe and Wolf-Gladrow, 2001). Simultaneously, the loss of 1 mole of CO_3^{2-} ions decrease the DIC concentration by 1 mole. Hence, any loss of TA and DIC following a 2:1 ratio can be linked to $CaCO_3$ precipitation (Zeebe and Wolf-Gladrow, 2001). Additionally, when $CaCO_3$ precipitation was suspected in our experiments, SEM and particulate inorganic carbon samples were taken to confirm the presence of $CaCO_3$ and to identify which polymorphs were predominant. In the +250 µmol kg⁻¹ TA additions by CaO and $Ca(OH)_2$, both appeared to fully dissolve without inducing $CaCO_3$ precipitation, as TA and Ω_A quickly increased within minutes, similarly to what has been described in the literature (Chave and Suess, 1970; Rushdi et al., 1992), until reaching their respective maxima after about a day and remaining stable over weeks (Figure 1a and 1c, Figure 2a and 2c). A slight increase in DIC was observed over time as expected since atmospheric CO_2 was absorbed from the bottle headspace, created when 150 to 200 mL of solution were withdrawn at each sampling point. The measured TA increase was slightly below the theoretically expected increase, which is assumed to be due to a combination of impurities present (in the case of CaO, a significant fraction could be hydrated), and any loss of the finely ground material during the weighing and sieving process. On average, ~23% of alkalinity added was not detected in the experiments with CaO, and about 14% for the experiments using $Ca(OH)_2$ (Table 1, Figure 1 and Figure 2).

In contrast, in the +500 µmol kg⁻¹ TA additions by CaO and $Ca(OH)_2$, TA started decreasing after about one day following the observed initial increase. If this TA loss was through $CaCO_3$ precipitation, DIC should be reduced by half this amount. The measured TA and DIC losses were very close to this 2:1 ratio for both the CaO and $Ca(OH)_2$ experiments with a TA addition of 500 µmol kg⁻¹ (950:465 and 860:395 for CaO and $Ca(OH)_2$, respectively). This suggests that TA precipitated in the form of $CaCO_3$. The slight off-set can be explained by ingassing of CO_2 from the headspace which lowers the TA:DIC ratio, becoming visible only when precipitation ceases towards the end (Figure 1b). Another caveat is that the maximum increase in TA from full dissolution of CaO or $Ca(OH)_2$ cannot be measured in the presence of concurrent $CaCO_3$ precipitation. This is mostly evident in the +2000 µmol kg⁻¹ TA addition (Figure 4), where DIC decreases due to $CaCO_3$ precipitation, yet TA increases due to higher $Ca(OH)_2$ dissolution rates. This also explains why estimated PIC calculated from measured TA changes is

generally smaller than measured PIC concentrations (Table 2). In the experiment with 1M Na_2CO_3 and quartz particles, the measured TA-based PIC estimates were larger than the measured PIC. This difference is difficult to explain and could be possibly linked to the observed white layer on the bottle walls, indicative of $CaCO_3$ precipitation. In any case, while being a laboratory artefact, this has no practical consequences as in a natural setting the TA would eventually precipitate in the water column. In summary, trying to estimate $CaCO_3$ precipitation from measured changes in TA, without knowing how much TA was actually generated by full mineral dissolution or actual PIC measurements, might underestimate total precipitation.

4.2 The presence of mineral phases triggers "runaway $CaCO_3$ precipitation"

An important finding in our experiments was that whenever $CaCO_3$ precipitation was observed, it continued even if the solution dropped below an Ω_A of ~4-5, levels at which no precipitation were observed in the +250 µmol kg^{-1} TA addition experiments. Furthermore, in all these experiments, precipitation decreased and seemingly ceased at an Ω_A of ~1.8-2.0. Therefore, it appears that when $CaCO_3$ is initially precipitated, $CaCO_3$ continues to precipitate in a runaway fashion, even if Ω_A drops below levels where precipitation would not be initiated in natural seawater. This is to be expected as $CaCO_3$ precipitates onto $CaCO_3$ mineral surfaces at any saturation state above 1, and the initial precipitation at high saturation states provides new nucleation sites (Morse et al., 2007; Morse et al., 2003; Zhong and Mucci, 1989). Precipitation rate is directly proportional to Ω, decreasing exponentially until reaching zero at an Ω value of 1 (Figure A4). However, the question of why precipitation occurred at a much lower Ω than anticipated, i.e., Ω ~7.5 vs ~12.3, remains (Marion et al., 2009).

It is known that the presence of particles in suspension can initiate and accelerate $CaCO_3$ precipitation (Millero et al., 2001; Morse et al., 2003; Wurgaft et al., 2021). It is unlikely that the presence of $CaCO_3$ impurities in CaO (less than 1% carbon) and $Ca(OH)_2$ (less than 2% carbon) from imperfect calcination would have caused precipitation, as the presence of $CaCO_3$ mineral phases should have caused precipitation at any saturation state above 1, i.e., also in the +250 µmol kg^{-1} TA addition experiments. Furthermore, modelling precipitation using experimentally determined Ω_A and surface area dependant aragonite precipitation rates onto $CaCO_3$ mineral phases (Zhong and Mucci, 1989), suggests that once precipitation becomes analytically detectable, it should proceed very rapidly before levelling off (Figure A5). Furthermore, while we expected $CaCO_3$ precipitation to stop at an Ω_A ~1, we observed it to stop at Ω_A of ~2. The presence of dissolved organic carbon and soluble reactive phosphate could have slowed down if not stopped $CaCO_3$ precipitation at an Ω_A higher than 1 (Chave and Suess, 1970; Pan et al., 2021). We also observed that the bulk of precipitation occurred over a period of at least a week, after which an equilibration was reached with apparent differences between the different dissolving minerals (i.e., CaO, $Ca(OH)_2$ and quartz, although it is acknowledged that the experiments were not replicated).

Another explanation for $CaCO_3$ precipitation is heterogeneous precipitation on not yet dissolved CaO and $Ca(OH)_2$ particles (or other impurities), leading to $CaCO_3$ crystal formation and initiating runaway precipitation. The Ω_A threshold for this process would depend on lattice compatibility of the mineral phases (Tang et al., 2020). For instance, $CaCO_3$ precipitation has been observed at any saturation state above 1 when introducing $CaCO_3$ seed particles. In contrast, Lioliou et al. (2007) did not report $CaCO_3$ precipitation onto quartz particles at an Ω_A lower than 3.5, and in order to trigger $CaCO_3$ precipitation onto

quartz particles, Ω_A would need to be further increased. Here, we observed $CaCO_3$ precipitation on quartz particles at an Ω_A of ~9.2 (Figure 3). The reason for an initially slower but then more rapid precipitation could be a combination of exponentially increasing $CaCO_3$ surface area, while increasing lattice compatibility (Lioliou et al., 2007; Pan et al., 2021). The filtration of TA-enriched seawater supports this idea, since not yet dissolved mineral phases that could facilitate early nucleation were removed, preventing runaway $CaCO_3$ precipitation (Figure 3).

Needle-shaped aragonite precipitation onto quartz particles (Figure 5c and 5d) was observed by SEM imaging. EDX analyses identified the larger mineral to be rich in silicon, a key characteristic of quartz, and the needle-shaped particles composed of carbon, oxygen and calcium, indicative for $CaCO_3$ (Chang et al., 2017; Ni and Ratner, 2008; Pan et al., 2021). In contrast, direct aragonite precipitation onto not yet dissolved CaO and $Ca(OH)_2$ in the +500 µmol kg^{-1} TA addition is difficult to prove as EDX analyses revealed the presence of Ca and O in both the mineral feedstocks and aragonite (Figure 5a and 5b). Finally, in some situations (Figure 5b), round crystals were also observed, suggesting the presence of vaterite (Chang et al., 2017). Nevertheless, aragonite crystals represented the majority of $CaCO_3$ observed by SEM.

4.3 Impacts of $CaCO_3$ precipitation on OAE potential

From an OAE perspective, $CaCO_3$ precipitation is an important chemical reaction that needs to be avoided. During $CaCO_3$ precipitation, dissolved $[CO_3^{2-}]$ and Ω decrease, and $[CO_2]$ increases, which reduces the ocean's uptake capacity for atmospheric CO_2, hence impacting the OAE potential. Considering typical open ocean TA and DIC concentrations of 2350 and 2100 µmol kg^{-1} respectively, at a salinity of 35 and a temperature of 19 °C, this water mass would have a pCO_2 close to atmospheric equilibrium of 416 µatm, a pH_T value (total scale) of 8.04, and an Ω_A of 2.80. Without $CaCO_3$ precipitation, an addition of 500 µmol kg^{-1} TA would lower pCO_2 to ~92 µatm while increasing pH_T and Ω_A to about 8.61 and 8.45, respectively. If fully re-equilibrated with the atmosphere, DIC would increase by about 420 µmol kg^{-1}, leading to a pH_T and Ω_A, respectively, 0.07 and 1.10 higher than prior to the addition (Table 3). The resulting OAE efficiency would be 0.83 mole of atmospheric CO_2 absorbed per mole of TA added, very similar to estimates by Köhler et al. (2010). Considering that $CaCO_3$ is the source material for CaO and $Ca(OH)_2$, and that 2 moles of TA are produced per mole of CaO or $Ca(OH)_2$ mineral dissolution, ~0.7 tonnes of CO_2 could be captured per tonne of source material, assuming CO_2 capture during the calcination process. At a global-scale, using all available ship capacity and assuming a slow discharge of 1.7 to 4.0 Gt of $Ca(OH)_2$ per year (Caserini et al., 2021), between 1.2 and 2.8 Gt of CO_2 per year could be absorbed by the ocean. Including direct coastal TA discharge at a constant addition of $Ca(OH)_2$ of 10 Gt year^{-1} (Feng et al., 2016), we could expect to absorb an additional 7 Gt of CO_2 per year. To put these model-derived numbers into perspective, the global cement industry currently produces about 4.1 Gt of cement per year (Statista, 2021). Depending on whether hydraulic ($4CaO \cdot Al_2O_3 \cdot Fe_2O_3$) or non-hydraulic ($Ca(OH)_2$) cement is being produced, and assuming a molar Ca^{2+} to CO_2 sequestration potential of 1.6, up to 3.9 Gt of atmospheric CO_2 could be captured per year. This is within the range required over the next 30 years to keep global warming below the 2 °C target, as in the shared socioeconomic pathway RCP2.6 scenario (Huppmann et al., 2018).

14

The above numbers can only be achieved if CaO or Ca(OH)$_2$ dissolution is complete without CaCO$_3$ precipitation. Hypothetically, when as much CaCO$_3$ precipitates as TA is added, i.e., 100 µmol kg^{-1} of CaCO$_3$ precipitate after a TA increase of 100 µmol kg^{-1}, only 1 instead of 1.6 moles of DIC can be absorbed per 2 moles of TA, after equilibration with atmospheric pCO$_2$ (Table 3). This represents a decrease by nearly 40% in OAE potential. Similarly, runaway CaCO$_3$ precipitation until an Ω_A of 2.0, as observed here, decreases the OAE potential further by almost 90%. Consequently, only ~0.1 mole of DIC would be absorbed per mole of TA added (Table 3). Furthermore, secondary CaCO$_3$ precipitation higher than TA addition will lead to pH$_T$ and Ω levels lower than the initial ones. For instance, runaway precipitation for a TA addition of 500 µmol kg^{-1} will see pH$_T$ drop by about 0.1 from 8.04 to 7.93 and Ω_A from 2.80 to 1.66, significantly enhancing ongoing ocean acidification (Table 3). Runaway CaCO$_3$ precipitation for a TA addition of 1000 µmol kg^{-1} (assumed to cease at an Ω_A of 2 as observed here) would see a further drop in Ω_A, i.e., to below 1, upon CO$_2$ re-equilibration with the atmosphere (Table 3). Under such conditions, aragonite would start to dissolve, impacting various marine organisms, especially carbonate-secreting organisms, e.g., sessile corals, benthic molluscs and planktonic pteropods (Riebesell et al., 2011; Zeebe and Wolf-Gladrow, 2001). In summary, runaway CaCO$_3$ precipitation in OAE must be avoided as it will not only reduce CO$_2$ uptake efficiency significantly but also enhance ocean acidification. Keeping track of OAE efficiency from changes in TA concentrations can be challenging as CaCO$_3$ precipitation can be underestimated as described earlier, requiring new and clever monitoring strategies.

4.4 Avoiding CaCO$_3$ precipitation by dilution and other TA addition strategies

An important aspect when it comes to avoiding CaCO$_3$ precipitation is the dilution that would occur in the wake of ships releasing TA in the ocean, or by natural mixing of TA-enriched water with surrounding seawater (Caserini et al., 2021; Feng et al., 2017; Mongin et al., 2021). In our experiments, a 1:1 dilution appeared to seemingly inhibit CaCO$_3$ precipitation in seawater, even if performed only after one week for the +500 µmol kg^{-1} TA addition. At a first glance, this comes as a surprise since precipitation nuclei would only be diluted by half, reducing surface area and precipitation rates by a factor of 2. However, as Ω_A is simultaneously reduced, precipitation rates are further reduced by a factor of 10 (see Figure A4). Hence, overall precipitation rate would see a reduction by a factor of 20. This should slow down precipitation initiated upon the alkalinity addition, if on CaCO$_3$ particles, but not completely inhibit it (Zhong and Mucci, 1989). A possible explanation could be that dilution lowers Ω_A below the critical threshold, overcoming the lattice mismatch, as most of the aragonite precipitation appears to be on the original seed mineral itself rather than on the newly formed aragonite (compare Figure 5c and 5d).

Overall, CaCO$_3$ precipitation can be avoided if the TA+500 µmol kg^{-1} enriched seawater is diluted 1:1, reaching an Ω_A of ~5.0. The quicker dilution takes place, the less CaCO$_3$ would precipitate prior to dilution. Similar results were found for a TA addition of +2000 µmol kg^{-1}, i.e., the ability to stop precipitation at an Ω_A of ~5.0, after a 1:7 dilution. However, only the 10-minute and 1-hour dilutions seem to be suitable in an OAE context, as rapid aragonite precipitation at a higher initial Ω_A of about 16.7 would significantly reduce the CO$_2$ uptake efficiency. Furthermore, the difficulty in monitoring precipitation from simple TA measurements (as described above) would also mean that quantification of CO$_2$ removal is not straight-forward.

15

Therefore, in order to assign carbon credits, TA additions have to be done in a way that rule out or at least minimise secondary $CaCO_3$ precipitation. This is true for any type of TA addition, and is not specific to additions of quick and hydrated lime.

470   Adding TA from land, as modelled by Feng et al. (2017), shows that as more TA is added, higher coastal Ω_A would be reached. By staying well below the Ω_A threshold identified here, i.e., limiting coastal Ω_A to only 3.2, up to ~550 Gt of carbon in the form of CO_2 could be removed from the atmosphere between 2020 and 2100, corresponding to a reduction by about 260 ppm (Feng et al., 2017). The critical Ω_A threshold beyond which secondary $CaCO_3$ precipitation occurs could be higher for other alkaline minerals of interest for OAE, theoretically allowing for higher TA additions. However, it has to be kept in mind

475   that in waters with high sediment load, often found in coastal settings, $CaCO_3$ could precipitate onto other mineral particles than those added to increase TA. This has been observed in river plumes (Wurgaft et al., 2021), on resuspended sediments of the Bahama Banks (Bustos-Serrano et al., 2009) and in the Red Sea following flash flood deposition of resuspended sediments and particles (Wurgaft et al., 2016). Even with minerals allowing for higher TA additions, an Ω_A threshold of 5 might be safer to adopt. Atmospheric CO_2 removal could be increased if TA would also be added to the open ocean, e.g., on ships of

480   opportunity. Here, additions could be much higher as ship movement and rapid mixing within its wake would significantly dilute added TA as opposed to coastal point sources (Caserini et al., 2021; Köhler et al., 2013).

        Finally, another option to increase atmospheric CO_2 uptake would be to keep the seawater equilibrated with air or CO_2-enriched flue gases, during mineral dissolution. Firstly, an Ω_A of 3.3 would be reached as opposed to 5 in the +250 µmol kg^{-1} TA scenario (Table 3), when equilibration occurs during instead of after the dissolution process. Secondly, when reaching an

485   Ω_A of 5 with CO_2 equilibration, nearly 1000 instead of 250 µmol kg^{-1} of TA could be added, allowing for almost 4 times the amount of atmospheric CO_2 to be removed (this number is highly sensitive to temperature, and ranges between ~3 and ~6 between 30 and 5 °C). Unfortunately, this requires an extra step, which appears to be far more time consuming and costly than a simple mineral addition. It should also be kept in mind that for the same Ω_A threshold, the amount of TA that can be added will increase at lower temperatures, because of higher CO_2 solubility and, hence, naturally lower Ω_A in colder waters. Based

490   on our Ω_A threshold of 5, at a salinity of 35 and at 5 °C, about three times as much TA can be dissolved than at 30 °C.

5 Conclusions

        OAE is a negative emission technology with a large potential for atmospheric CO_2 removal (Caserini et al., 2021; Feng et al., 2016; Köhler et al., 2010). In order to maximise CO_2 uptake efficiency, secondary $CaCO_3$ precipitation has to be avoided. Here we show that an increase of TA by 500 µmol kg^{-1} led to aragonite precipitation, reducing the CO_2 uptake

495   potential from about 0.8 mole per mole of TA added to nearly 0.1 mole. Precipitation most likely occurred on the CaO and $Ca(OH)_2$ mineral surfaces prior to their full dissolution. In contrast, an addition of 250 µmol kg^{-1} of TA did not result in $CaCO_3$ precipitation, suggesting that an Ω_A of about 5 is a safe limit. This is probably the case for other minerals with even lower lattice compatibility for $CaCO_3$, since $CaCO_3$ could precipitate onto naturally present mineral phases in coastal settings, such as resuspended sediments. Safely increasing the amount of TA that could be added to the ocean could be achieved by 1)

500 allowing for major mixing and dilution of enriched seawater by coastal tides or in the wake of ships, 2) equilibrating the seawater to atmospheric CO_2 levels prior to the addition during mineral dissolution, and/or 3) targeting low rather than high temperature regions.

Data availability

Data will be made available on a publicly available repository upon final publication.

Author contributions

505 CAM and KGS designed the initial experiments. All co-authors contributed to the initial data analysis and design of follow-up experiments. CAM performed most of the sampling, and the data analyses with the help of KGS. CAM wrote the paper with KGS, with inputs from all the co-authors.

Competing interests

510 The authors declare that they have no conflict of interest.

520

References

Bach, L. T., Gill, S., Rickaby, R., Gore, S., and Renforth, P.: CO2 removal with enhanced weathering and ocean alkalinity enhancement: Potential risks and co-benefits for marine pelagic ecosystems, Frontiers in Climate, 1, 7, 2019.

Bates, N., Best, M., Neely, K., Garley, R., Dickson, A., and Johnson, R.: Detecting anthropogenic carbon dioxide uptake and ocean acidification in the North Atlantic Ocean, Biogeosciences Discussions, 9, 2012.

Boyd, P., Vivian, C., Boettcher, M., Chai, F., Cullen, J., Goeschl, T., Lampitt, R., Lenton, A., Oschlies, A., and Rau, G.: High level review of a wide range of proposed marine geoengineering techniques, 2019.

Burt, D. J., Fröb, F., and Ilyina, T.: The sensitivity of the marine carbonate system to regional ocean alkalinity enhancement, Frontiers in Climate, 3, 2021.

Bustos-Serrano, H., Morse, J. W., and Millero, F. J.: The formation of whitings on the Little Bahama Bank, Marine Chemistry, 113, 1-8, 2009.

Canadell, J. G., Le Quéré, C., Raupach, M. R., Field, C. B., Buitenhuis, E. T., Ciais, P., Conway, T. J., Gillett, N. P., Houghton, R., and Marland, G.: Contributions to accelerating atmospheric CO2 growth from economic activity, carbon intensity, and efficiency of natural sinks, Proceedings of the national academy of sciences, 104, 18866-18870, 2007.

Carter, B. R., Feely, R. A., Wanninkhof, R., Kouketsu, S., Sonnerup, R. E., Pardo, P. C., Sabine, C. L., Johnson, G. C., Sloyan, B. M., and Murata, A.: Pacific anthropogenic carbon between 1991 and 2017, Global Biogeochemical Cycles, 33, 597-617, 2019.

Caserini, S., Pagano, D., Campo, F., Abbà, A., De Marco, S., Righi, D., Renforth, P., and Grosso, M.: Potential of Maritime Transport for Ocean Liming and Atmospheric CO2 Removal, Frontiers in Climate, 3, 22, 2021.

Chang, R., Kim, S., Lee, S., Choi, S., Kim, M., and Park, Y.: Calcium carbonate precipitation for CO2 storage and utilization: a review of the carbonate crystallization and polymorphism, Frontiers in Energy Research, 5, 17, 2017.

Chave, K. E. and Suess, E.: Calcium Carbonate Saturation in Seawater: Effects of Dissolved Organic Matter 1, Limnology and Oceanography, 15, 633-637, 1970.

Chen, T., Neville, A., and Yuan, M.: Calcium carbonate scale formation—assessing the initial stages of precipitation and deposition, Journal of Petroleum Science and Engineering, 46, 185-194, 2005.

Cyronak, T., Schulz, K. G., Santos, I. R., and Eyre, B. D.: Enhanced acidification of global coral reefs driven by regional biogeochemical feedbacks, Geophysical Research Letters, 41, 5538-5546, 2014.

De Choudens-Sanchez, V. and Gonzalez, L. A.: Calcite and aragonite precipitation under controlled instantaneous supersaturation: elucidating the role of CaCO3 saturation state and Mg/Ca ratio on calcium carbonate polymorphism, Journal of Sedimentary Research, 79, 363-376, 2009.

Dickson, A. and Millero, F. J.: A comparison of the equilibrium constants for the dissociation of carbonic acid in seawater media, Deep Sea Research Part A. Oceanographic Research Papers, 34, 1733-1743, 1987.

Dickson, A. G.: Standards for ocean measurements, Oceanography, 23, 34-47, 2010.

Dickson, A. G., Sabine, C. L., and Christian, J. R.: Guide to best practices for ocean CO2 measurements, North Pacific Marine Science Organization, 2007.

Doney, S. C., Fabry, V. J., Feely, R. A., and Kleypas, J. A.: Ocean acidification: the other CO2 problem, Annual review of marine science, 1, 169-192, 2009.

Feng, E., Koeve, W., Keller, D. P., and Oschlies, A.: Model-Based Assessment of the CO2 Sequestration Potential of Coastal Ocean Alkalinization, Earth's Future, 5, 1252-1266, 2017.

Feng, E. Y., Keller, D. P., Koeve, W., and Oschlies, A.: Could artificial ocean alkalinization protect tropical coral ecosystems from ocean acidification?, Environmental Research Letters, 11, 074008, 2016.

Friedlingstein, P., Jones, M. W., O'Sullivan, M., Andrew, R. M., Bakker, D. C., Hauck, J., Le Quéré, C., Peters, G. P., Peters, W., and Pongratz, J.: Global carbon budget 2021, Earth System Science Data, 14, 1917-2005, 2022.

Gafar, N. A. and Schulz, K. G.: A three-dimensional niche comparison of Emiliania huxleyi and Gephyrocapsa oceanica: reconciling observations with projections, Biogeosciences, 15, 3541-3560, 2018.

Gattuso, J.-P., Magnan, A., Billé, R., Cheung, W. W., Howes, E. L., Joos, F., Allemand, D., Bopp, L., Cooley, S. R., and Eakin, C. M.: Contrasting futures for ocean and society from different anthropogenic CO2 emissions scenarios, Science, 349, aac4722, 2015.

González, M. F. and Ilyina, T.: Impacts of artificial ocean alkalinization on the carbon cycle and climate in Earth system simulations, Geophysical Research Letters, 43, 6493-6502, 2016.

Goodwin, P., Brown, S., Haigh, I. D., Nicholls, R. J., and Matter, J. M.: Adjusting mitigation pathways to stabilize climate at 1.5 C and 2.0 C rise in global temperatures to year 2300, Earth's Future, 6, 601-615, 2018.

Harvey, L.: Mitigating the atmospheric CO2 increase and ocean acidification by adding limestone powder to upwelling regions, Journal of Geophysical Research: Oceans, 113, 2008.

Hoegh-Guldberg, O., Jacob, D., Taylor, M., Bolaños, T. G., Bindi, M., Brown, S., Camilloni, I., Diedhiou, A., Djalante, R., and Ebi, K.: The human imperative of stabilizing global climate change at 1.5° C, Science, 365, eaaw6974, 2019.

Hoegh-Guldberg, O., Mumby, P. J., Hooten, A. J., Steneck, R. S., Greenfield, P., Gomez, E., Harvell, C. D., Sale, P. F., Edwards, A. J., and Caldeira, K.: Coral reefs under rapid climate change and ocean acidification, science, 318, 1737-1742, 2007.

Huppmann, D., Kriegler, E., Krey, V., Riahi, K., Rogelj, J., Rose, S. K., Weyant, J., Bauer, N., Bertram, C., and Bosetti, V.: IAMC 1.5 C Scenario Explorer and Data hosted by IIASA, Integrated Assessment Modeling Consortium & International Institute for Applied Systems Analysis, 10, 2018.

Ilyina, T., Wolf-Gladrow, D., Munhoven, G., and Heinze, C.: Assessing the potential of calcium-based artificial ocean alkalinization to mitigate rising atmospheric CO2 and ocean acidification, Geophysical Research Letters, 40, 5909-5914, 2013.

IPCC: Summary for Policymakers. In: Climate Change 2021: The Physical Science Basis. Contribution of Working Group I to the Sixth Assessment Report of the Intergovernmental Panel on Climate Change [Masson-Delmotte, V., P. Zhai, A. Pirani, S. L. Connors, C. Péan, S. Berger, N. Caud, Y. Chen, L. Goldfarb, M. I. Gomis, M. Huang, K. Leitzell, E. Lonnoy, J.B.R. Matthews, T. K. Maycock, T. Waterfield, O. Yelekçi, R. Yu and B. Zhou (eds.)]. Cambridge University Press. In Press., 2021.

Keller, D. P., Feng, E. Y., and Oschlies, A.: Potential climate engineering effectiveness and side effects during a high carbon dioxide-emission scenario, Nature communications, 5, 1-11, 2014.

Kheshgi, H. S.: Sequestering atmospheric carbon dioxide by increasing ocean alkalinity, Energy, 20, 915-922, 1995.

Köhler, P., Hartmann, J., and Wolf-Gladrow, D. A.: Geoengineering potential of artificially enhanced silicate weathering of olivine, Proceedings of the National Academy of Sciences, 107, 20228-20233, 2010.

Köhler, P., Abrams, J. F., Völker, C., Hauck, J., and Wolf-Gladrow, D. A.: Geoengineering impact of open ocean dissolution of olivine on atmospheric CO2, surface ocean pH and marine biology, Environmental Research Letters, 8, 014009, 2013.

Lenton, A., Matear, R. J., Keller, D. P., Scott, V., and Vaughan, N. E.: Assessing carbon dioxide removal through global and regional ocean alkalinization under high and low emission pathways, Earth System Dynamics, 9, 339-357, 2018.

Lenton, T. and Vaughan, N.: The radiative forcing potential of different climate geoengineering options. Atmos. Chem. Phys. Discuss., V, 2009.

Lewis, E. and Perkin, R.: The practical salinity scale 1978: conversion of existing data, Deep Sea Research Part A. Oceanographic Research Papers, 28, 307-328, 1981.

Lioliou, M. G., Paraskeva, C. A., Koutsoukos, P. G., and Payatakes, A. C.: Heterogeneous nucleation and growth of calcium carbonate on calcite and quartz, Journal of colloid and interface science, 308, 421-428, 2007.

Lueker, T. J., Dickson, A. G., and Keeling, C. D.: Ocean pCO2 calculated from dissolved inorganic carbon, alkalinity, and equations for K1 and K2: validation based on laboratory measurements of CO2 in gas and seawater at equilibrium, Marine chemistry, 70, 105-119, 2000.

Marion, G., Millero, F. J., and Feistel, R.: Precipitation of solid phase calcium carbonates and their effect on application of seawater SA–T–P models, Ocean Science, 5, 285, 2009.

Mehrbach, C., Culberson, C., Hawley, J., and Pytkowicx, R.: Measurement of the apparent dissociation constants of carbonic acid in seawater at atmospheric pressure 1, Limnology and oceanography, 18, 897-907, 1973.

Millero, F., Huang, F., Zhu, X., Liu, X., and Zhang, J.-Z.: Adsorption and desorption of phosphate on calcite and aragonite in seawater, Aquatic Geochemistry, 7, 33-56, 2001.

Mongin, M., Baird, M. E., Lenton, A., Neill, C., and Akl, J.: Reversing ocean acidification along the Great Barrier Reef using alkalinity injection, Environmental Research Letters, 16, 064068, 2021.

Montserrat, F., Renforth, P., Hartmann, J., Leermakers, M., Knops, P., and Meysman, F. J.: Olivine dissolution in seawater: implications for CO2 sequestration through enhanced weathering in coastal environments, Environmental science & technology, 51, 3960-3972, 2017.

Morse, J. W. and He, S.: Influences of T, S and PCO2 on the pseudo-homogeneous precipitation of CaCO3 from seawater: implications for whiting formation, Marine Chemistry, 41, 291-297, 1993.

620   Morse, J. W., Arvidson, R. S., and Lüttge, A.: Calcium carbonate formation and dissolution, Chemical reviews, 107, 342-381, 2007.

Morse, J. W., Gledhill, D. K., and Millero, F. J.: Caco3 precipitation kinetics in waters from the great Bahama bank:: Implications for the relationship between bank hydrochemistry and whitings, Geochimica et Cosmochimica Acta, 67, 2819-2826, 2003.

625   Morse, J. W., Wang, Q., and Tsio, M. Y.: Influences of temperature and Mg: Ca ratio on CaCO3 precipitates from seawater, Geology, 25, 85-87, 1997.

Mucci, A.: The solubility of calcite and aragonite in seawater at various salinities, temperatures, and one atmosphere total pressure, Am. J. Sci, 283, 780-799, 1983.

National Academies of Sciences, E. and Medicine: A Research Strategy for Ocean-based Carbon Dioxide Removal and
630   Sequestration, The National Academies Press, Washington, DC, 360 pp., doi:10.17226/26278, 2021.

Ni, M. and Ratner, B. D.: Differentiating calcium carbonate polymorphs by surface analysis techniques—an XPS and TOF-SIMS study, Surface and Interface Analysis: An International Journal devoted to the development and application of techniques for the analysis of surfaces, interfaces and thin films, 40, 1356-1361, 2008.

Pan, Y., Li, Y., Ma, Q., He, H., Wang, S., Sun, Z., Cai, W.-J., Dong, B., Di, Y., and Fu, W.: The role of Mg2+ in inhibiting
635   CaCO3 precipitation from seawater, Marine Chemistry, 104036, 2021.

Pytkowicz, R. M.: Rates of inorganic calcium carbonate nucleation, The Journal of Geology, 73, 196-199, 1965.

Renforth, P. and Henderson, G.: Assessing ocean alkalinity for carbon sequestration, Reviews of Geophysics, 55, 636-674, 2017.

Renforth, P. and Kruger, T.: Coupling mineral carbonation and ocean liming, Energy & fuels, 27, 4199-4207, 2013.

640   Renforth, P., Jenkins, B., and Kruger, T.: Engineering challenges of ocean liming, Energy, 60, 442-452, 2013.

Riebesell, U., Fabry, V. J., Hansson, L., and Gattuso, J.-P.: Guide to best practices for ocean acidification research and data reporting, Office for Official Publications of the European Communities2011.

Riley, J. and Tongudai, M.: The major cation/chlorinity ratios in sea water, Chemical Geology, 2, 263-269, 1967.

Rushdi, A., Pytkowicz, R., Suess, E., and Chen, C.: The effects of magnesium-to-calcium ratios in artificial seawater, at
645   different ionic products, upon the induction time, and the mineralogy of calcium carbonate: a laboratory study, Geologische Rundschau, 81, 571-578, 1992.

Schulz, K. G., Bach, L. T., Bellerby, R. G., Bermúdez, R., Büdenbender, J., Boxhammer, T., Czerny, J., Engel, A., Ludwig, A., and Meyerhöfer, M.: Phytoplankton blooms at increasing levels of atmospheric carbon dioxide: experimental evidence for negative effects on prymnesiophytes and positive on small picoeukaryotes, Frontiers in Marine Science, 4, 64, 2017.

650   Simkiss, K.: The inhibitory effects of some metabolites on the precipitation of calcium carbonate from artificial and natural sea water, ICES Journal of Marine Science, 29, 6-18, 1964.

Statista: Global cement industry - Statistics & Facts. See: https://www.statista.com/topics/8700/cement-industry-worldwide/, 2021.

Tang, H., Wu, X., Xian, H., Zhu, J., Wei, J., Liu, H., and He, H.: Heterogeneous Nucleation and Growth of CaCO3 on Calcite
655   (104) and Aragonite (110) Surfaces: Implications for the Formation of Abiogenic Carbonate Cements in the Ocean, Minerals, 10, 294, 2020.

The Royal Society and Royal Academy of Engineering: Greenhouse Gas Removal. See: https://royalsociety.org/-/media/policy/projects/greenhouse-gas-removal/royal-society-greenhouse-gas-removal-report-2018.pdf, 2018.

Uppstrom, L.: The boron/chlorinity ratio of deep-sea water from the Pacific Ocean, Deep Sea Res., 21, 161-162, 1974.

660   Wolf-Gladrow, D. A., Zeebe, R. E., Klaas, C., Körtzinger, A., and Dickson, A. G.: Total alkalinity: The explicit conservative expression and its application to biogeochemical processes, Marine Chemistry, 106, 287-300, 2007.

Wolf, S. E., Leiterer, J., Kappl, M., Emmerling, F., and Tremel, W.: Early homogenous amorphous precursor stages of calcium carbonate and subsequent crystal growth in levitated droplets, Journal of the American Chemical Society, 130, 12342-12347, 2008.

665   Wurgaft, E., Steiner, Z., Luz, B., and Lazar, B.: Evidence for inorganic precipitation of CaCO3 on suspended solids in the open water of the Red Sea, Marine Chemistry, 186, 145-155, 2016.

Wurgaft, E., Wang, Z., Churchill, J., Dellapenna, T., Song, S., Du, J., Ringham, M., Rivlin, T., and Lazar, B.: Particle triggered reactions as an important mechanism of alkalinity and inorganic carbon removal in river plumes, Geophysical Research Letters, e2021GL093178, 2021.

670 Zeebe, R. E. and Wolf-Gladrow, D.: CO2 in seawater: equilibrium, kinetics, isotopes, 65, Gulf Professional Publishing2001.

Zhong, S. and Mucci, A.: Calcite and aragonite precipitation from seawater solutions of various salinities: Precipitation rates and overgrowth compositions, Chemical geology, 78, 283-299, 1989.

Table 1: Summary of experimental conditions. Please note that for comparability, more TA was added in the liquid than the sieved approaches to match the theoretical increases in calcium carbonate saturation state (see Methods section for details).

TA Agent	TA target (μmol kg^{-1})	Comments	Amount added in mg (or mL*)	Amount of natural seawater in kg	mg kg^{-1} (or mL* kg^{-1*})	Theoretical TA addition (μmol kg^{-1})	Recorded TA addition (μmol kg^{-1})	Experiment duration	Additional samples apart from TA and DIC
					Sieved calcium minerals experiments				
CaO	250	Sieved in	15.50	2.0159	7.69	274.21	216.49	47 days	N/A
CaO	500	Sieved in	30.60	2.0045	15.27	544.42	410.70	47 days	TPC, POC and SEM samples
Ca(OH)$_2$	250	Sieved in	19.90	2.001.9	9.94	268.34	221.96	28 days	N/A
Ca(OH)$_2$	500	Sieved in	37.40	2.0042	18.66	503.73	440.19	42 days	TPC, POC and SEM samples
					Na$_2$CO$_3$, particles and filtration experiments				
Na$_2$CO$_3$	1050	1M Na$_2$CO$_3$ solution	1.05*	2.0006	0.52	1050.32	1057.41	42 days	N/A
Na$_2$CO$_3$	1050	1M Na$_2$CO$_3$ solution, plus quartz powder after 2 days Sieved in,	1.05*	2.0003	0.5	1050.16	1073.92	48 days	TPC, POC and SEM samples
Ca(OH)$_2$	500	filtered after 4 hours	39.30	2.0043	19.61	529.30	470.79	48 days	N/A
					Dilution experiments				
Ca(OH)$_2$	500	1:1 dilution after 10min, 1 hour, 1 day and 1 week	101.60	5.1325	19.80	534.36	452.65	14 days	TPC, POC and SEM samples
Ca(OH)$_2$	2000	1:7 dilution after 10min, 1 hour, 1 day and 1 week	155.90	2.0038	77.80	2100.21	724.04	48 days	TPC, POC and SEM samples

675

Table 2: Comparison between the estimated PIC based on half the TA change between the theoretical maximum TA increase upon full dissolution of the alkaline material added and the measured TA at the end of the experiment (Table 1), the estimated PIC based on half the TA changes between the measured maximum TA increase and the measured TA at the end of the experiment, and the measured PIC from the particulate carbon analysis.
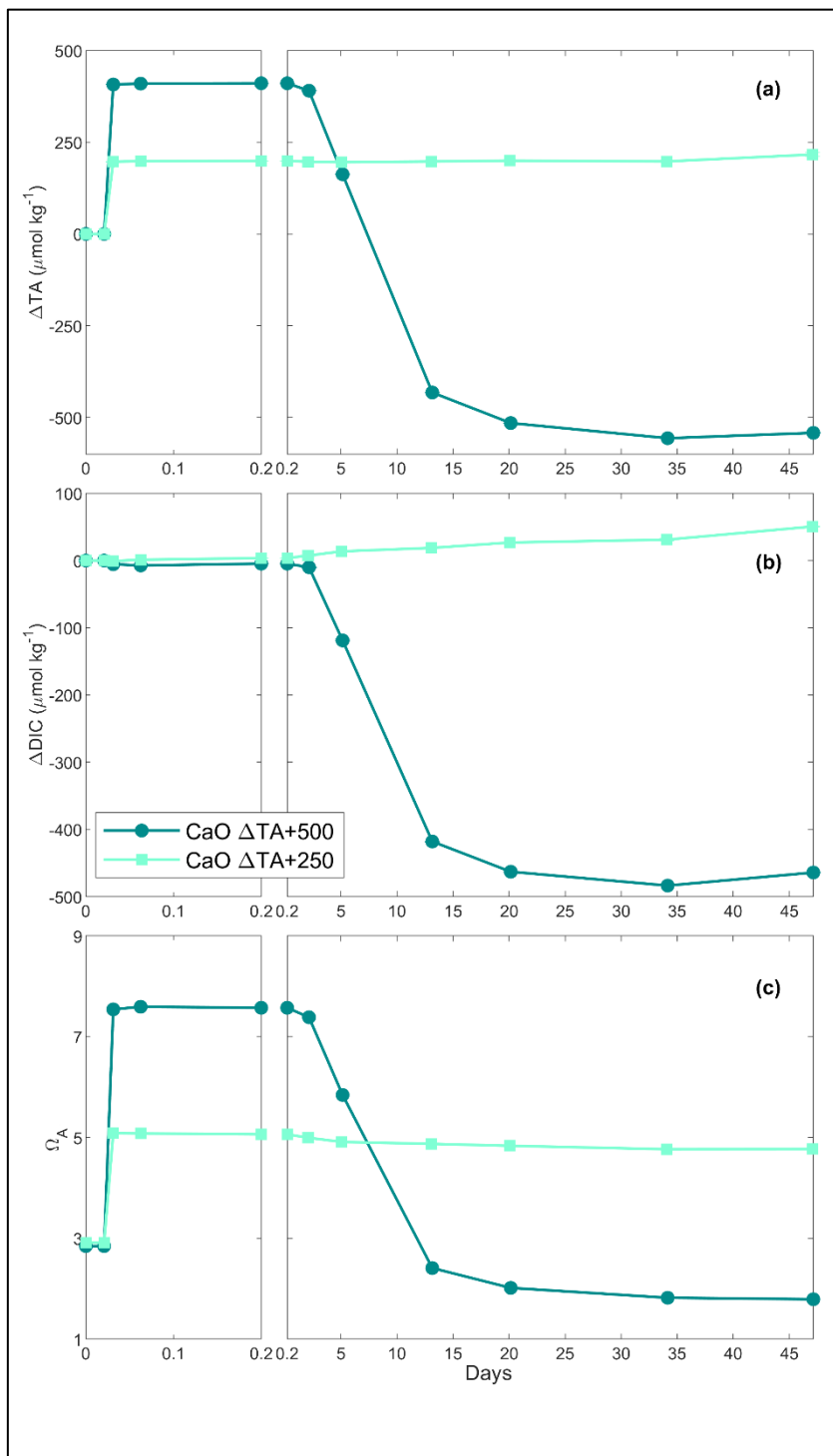
Experiment	PIC ΔTA_{Theo} ($\mu mol\ kg^{-1}$)	PIC ΔTA ($\mu mol\ kg^{-1}$)	Measured PIC ($\mu mol\ kg^{-1}$)
500 TA – CaO	543.24	476.38	491.82 ±39.18
500 TA – Ca(OH)$_2$	462.28	430.51	550.87 ±71.32
1050 TA – 1M Na$_2$CO$_3$+ Quartz Particles	627.20	639.07	397.37 ±24.03
500 TA – Ca(OH)$_2$ Dilution	107.05	66.20	89.51 ±4.27
2000 TA – Ca(OH)$_2$ Dilution	1718.83	1030.74	1331.48 ±50.73

Table 3: Simulations of the changes in TA, DIC, Ω_A, pCO_2 and pH_T (total scale) after TA increases of 250, 500 and 1000 µmol kg⁻¹, assuming complete mineral dissolution without precipitation, a complete dissolution followed by as much CaCO₃ precipitated as the amount of TA added, and a complete dissolution followed by CaCO₃ precipitation until reaching an Ω_A of 2.0, before CO₂ re-equilibration to initial pCO_2. For each scenario, the amount of moles of CO₂ absorbed per moles of TA added has been calculated for comparison. The 500 µmol kg⁻¹ TA addition simulation is shown in Figure A3, Appendix. *Note: the value for Ω_A is rounded to 1.00 but calculated at 0.997.

	Starting Conditions (salinity = 35 19 °C)	TA +250 µmol kg⁻¹ No CaCO₃ precipitation	TA +500 µmol kg⁻¹			TA +1000 µmol kg⁻¹		
			No CaCO₃ Prec.	CaCO₃ Prec. = TA added	CaCO₃ Prec. until Ω_A of 2	No CaCO₃ Prec.	CaCO₃ Prec. = TA added	CaCO₃ Prec. until Ω_A of 2
TA (µmol kg⁻¹)	2350	2600	2850	2350	1748	3350	2350	1320
DIC (µmol kg⁻¹)	2100	2100	2100	1850	1549	2100	1600	1085
Ω_A	2.80	5.53	8.45	5.34	2.00	14.57	7.89	2.00
pCO_2 (µatm)	416.2	175.1	91.5	135.6	319.2	29.6	48.2	144.81
pH_T	8.04	8.38	8.61	8.42	8.02	8.97	8.73	8.20
After re-equilibration, i.e., pCO_2 ~416 µatm								
Final TA (µmol kg⁻¹)	2350	2600	2850	2350	1748	3350	2350	1320
Final DIC (µmol kg⁻¹)	2100	2309	2517	2100	1588	2926.5	2100	1216
Final Ω_A	2.80	3.34	3.90	2.80	1.66	5.14	2.80	1.00*
Final pH_T	8.04	8.08	8.11	8.04	7.93	8.17	8.04	7.82
CO₂ uptake (mole/mole TA)	NA	0.84	0.83	0.50	0.08	0.83	0.50	0.13

Figure 1: Changes in TA (a), DIC (b) and Ω_A (c) over time following two CaO additions.

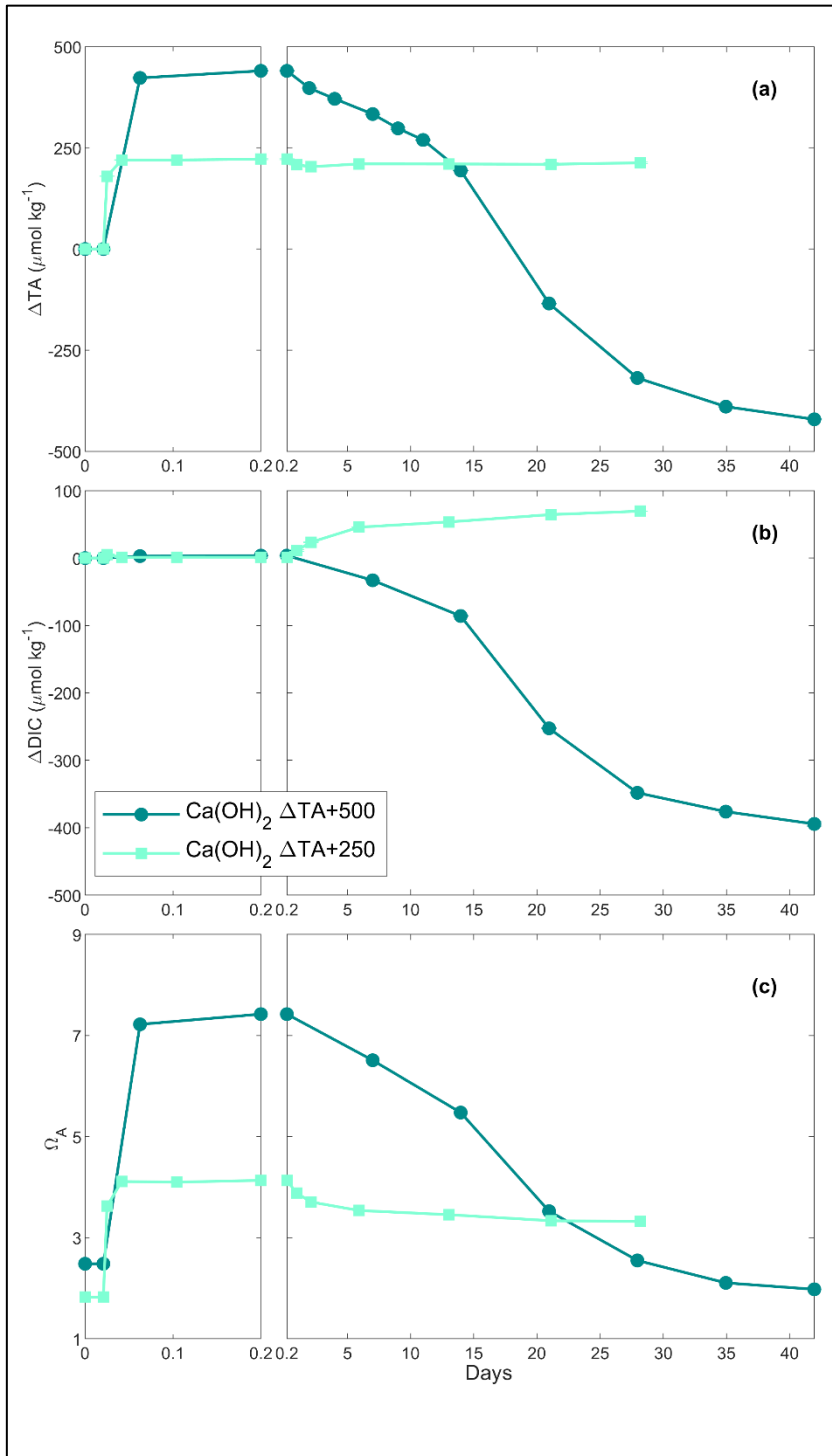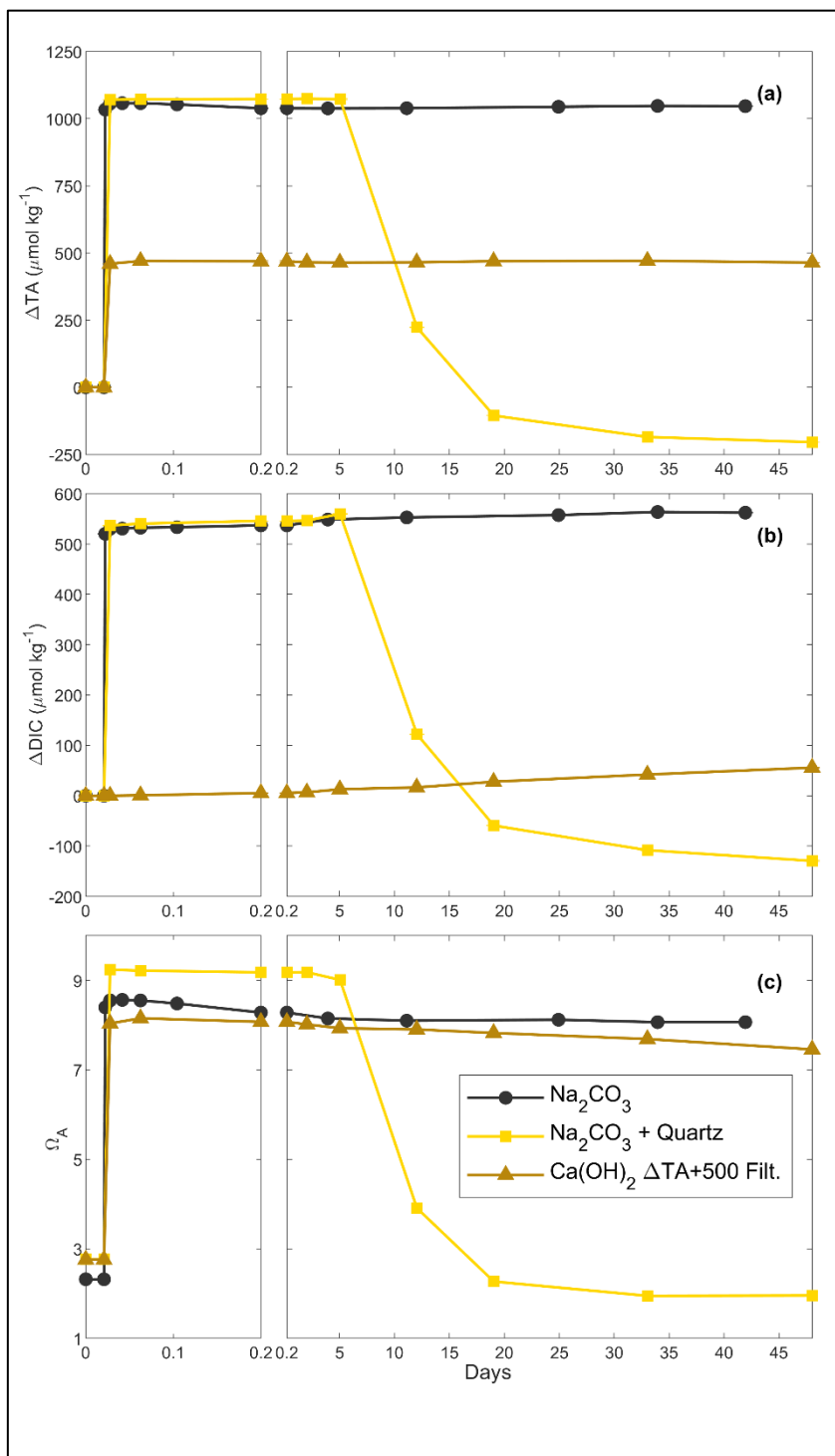**Figure 2: Changes in TA (a), DIC (b) and Ω_A (c) of the samples over time following two Ca(OH)$_2$ additions.**

Figure 3: Changes in TA (a), DIC (b) and Ω_A (c) over time following additions of Na$_2$CO$_3$, Na$_2$CO$_3$ plus quartz particles and Ca(OH)$_2$ followed by a filtration step (see Methods for details).
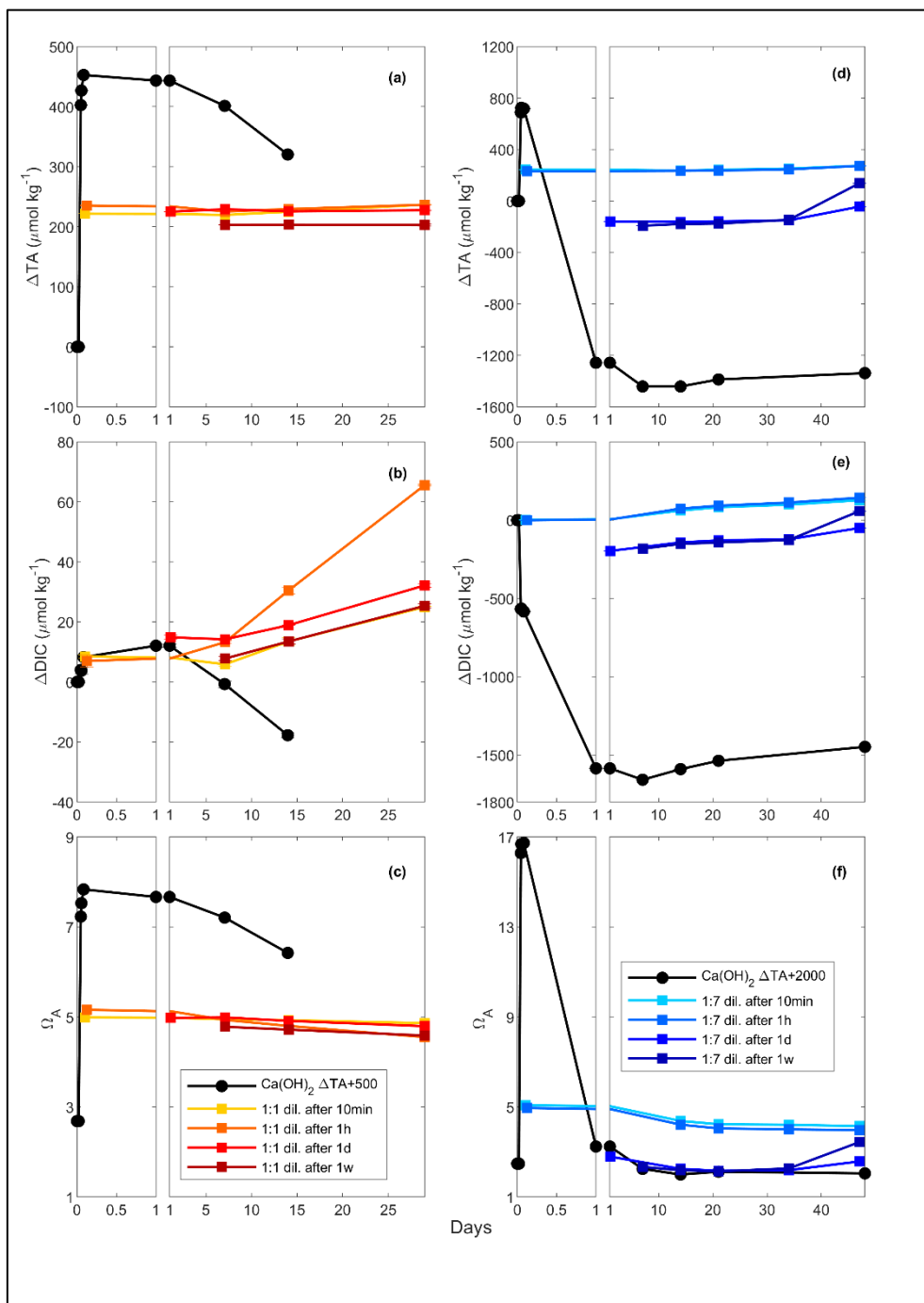
Figure 4: Changes in TA (a and d), DIC (b and e) and Ω_A (c and f) following a TA addition of 500 and 2000 µmol kg^{-1} respectively, by Ca(OH)$_2$ (black line), as well as following a 1:1 dilution or the 500 µmol kg^{-1} TA addition (red and yellow lines) and a 1:7 dilution for the 2000 µmol kg^{-1} TA addition (blue lines). The dilutions were performed after 10 minutes, 1 hour, 1 day and 1 week and earlier dilutions are represented by lighter colours.

700
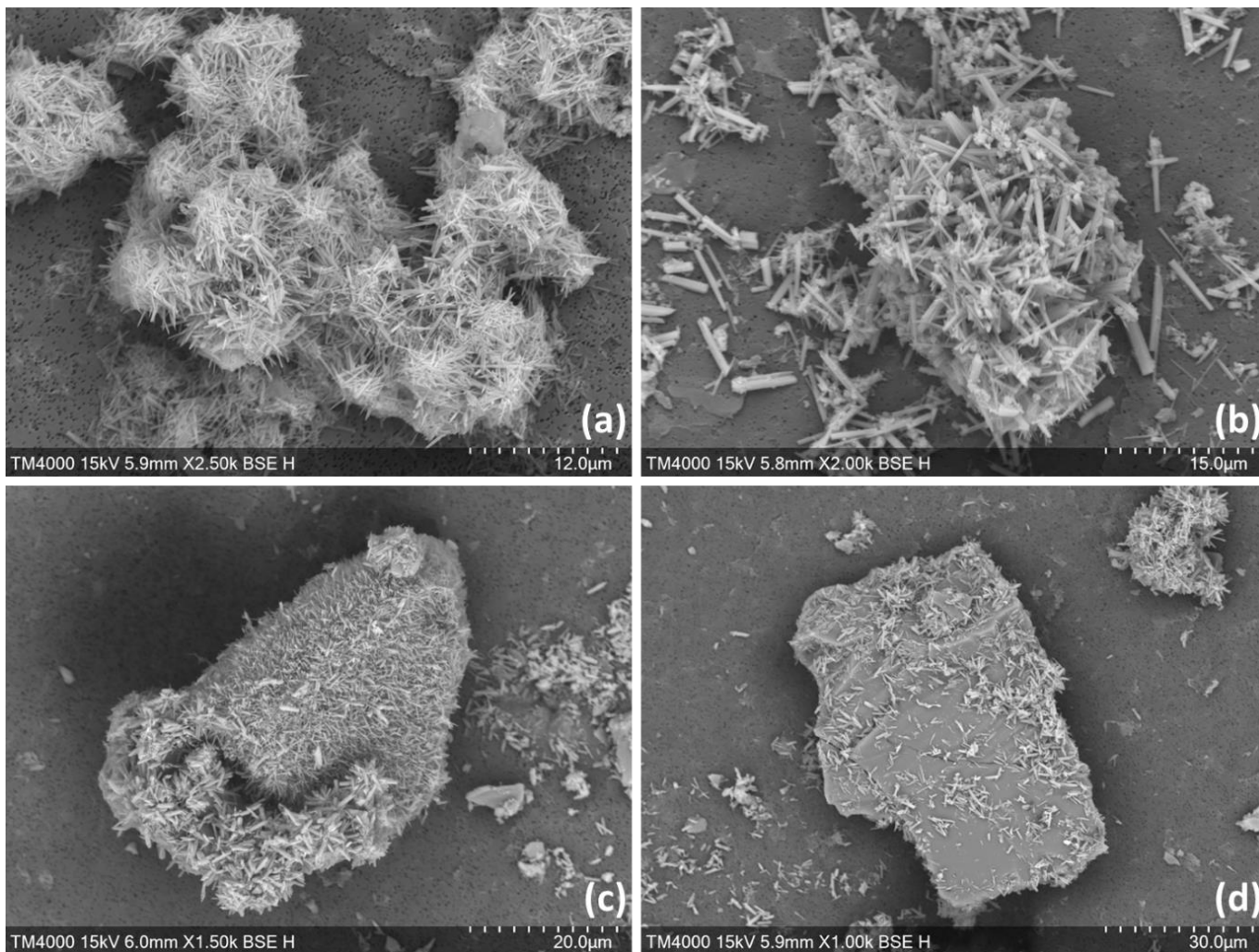
Figure 5: SEM images from experiments with an increase in TA of ~500 µmol kg^{-1} by CaO (a), Ca(OH)$_2$ (b) and with a TA increase of ~1050 µmol kg^{-1} by 1M Na$_2$CO$_3$, followed by quartz particles addition ((c) and (d)).

Appendix

Table A1: Seawater salinity in each experiment, and phosphate concentrations in one of the batches (*).

Alkaline mineral	TA increase (in μmol kg⁻¹)	Experiment details	Seawater salinity	Phosphate (in μmol kg⁻¹)*
CaO	250	N/A	36.52	Not measured
	500	N/A	36.52	Not measured
Ca(OH)$_2$	250	N/A	36.91	Not measured
	500	N/A	36.91	Not measured
	500	For dilutions	35.46	Not measured
	500	For filtration	36.52	Not measured
	2000	For dilution	36.74	0.32 ±0.03
Na$_2$CO$_3$	1050	N/A	36.91	Not measured
	1050	With quartz particles	36.52	Not measured

710

Table A2: Main chemical composition of the CaO and Ca(OH)$_2$ feedstocks used for the TA increase experiments determined by ICPMS analysis.

| CaO Powder			Ca(OH)$_2$ Powder		
Element	mg g⁻¹	St. Dev.	Element	mg g⁻¹	St. Dev.
Calcium	545.15	70.92	Calcium	529.79	117.30
Magnesium	2.10	0.23	Magnesium	6.87	1.98
Silicon	2.02	1.79	Silicon	2.70	1.12
Aluminium	0.50	0.19	Aluminium	1.98	0.77
Iron	0.32	0.10	Iron	0.91	0.34
Manganese	0.11	0.01	Potassium	0.43	0.23
Potassium	0.03	0.00	Titanium	0.07	0.03
Phosphorus	0.02	0.02	Manganese	0.05	0.01
Titanium	0.02	0.01	Phosphorus	0.04	0.01
Chromium	0.01	0.01	Bromine	0.03	0.01
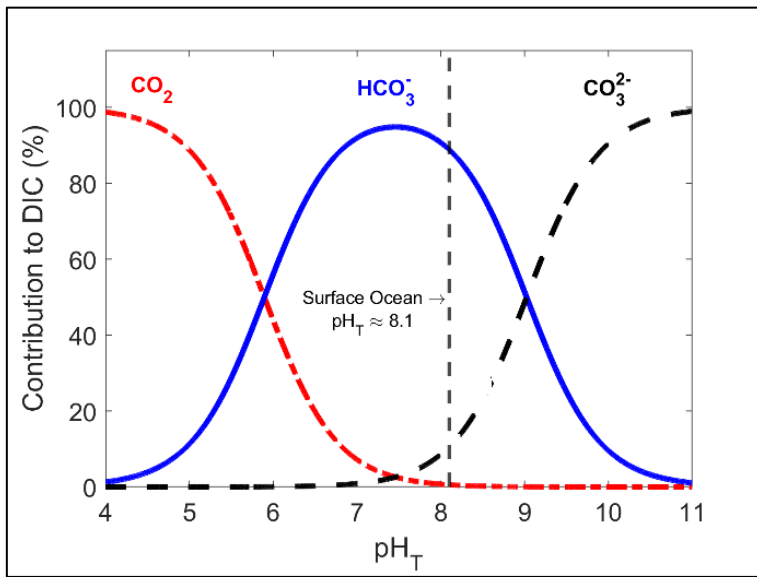
Figure A1: Relative contribution of dissolved CO_2, HCO_3^- and CO_3^{2-} to total dissolved inorganic carbon in seawater as a function of pH_T (total scale), also known as Bjerrum plot (based on the carbonic acid equilibrium constant from Mehrbach et al. (1973) and refitted by Dickson and Millero (1987)), at 25 °C and salinity of 35, with the current surface ocean pH average represented by the dashed line (pH_T ~8.1).
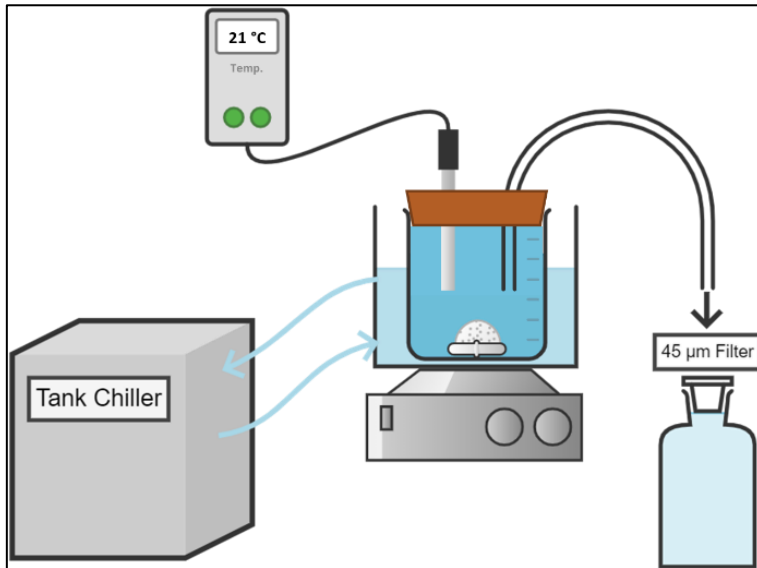
Figure A2: Conceptual diagram of the experimental setup used for the dissolution of alkaline minerals
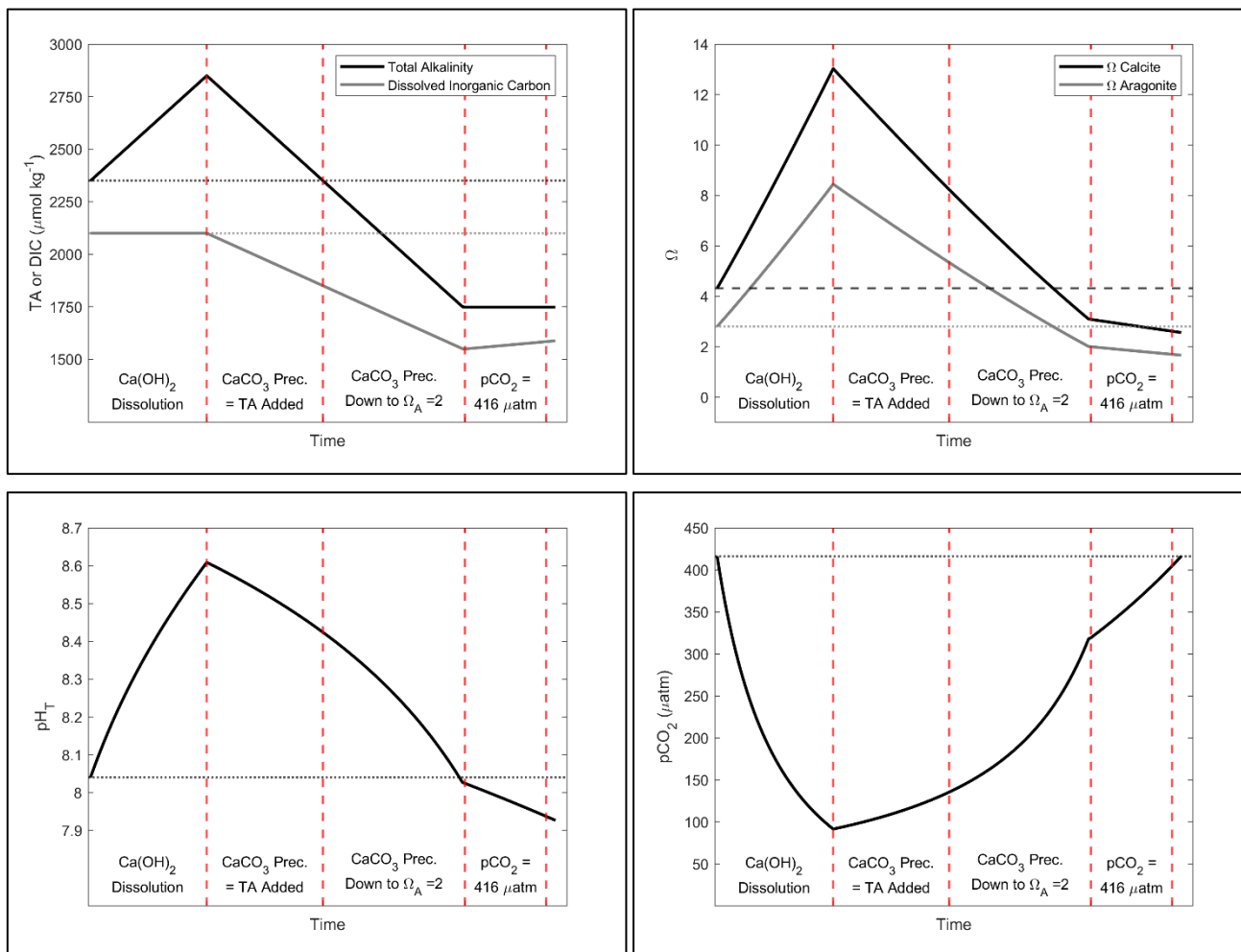
Figure A3: Simulation of the changes in TA, DIC, Ω_C, Ω_A, pCO$_2$ and pH$_T$ after addition of 500 µmol kg^{-1} of alkalinity. Four important steps are presented. First, assuming the complete Ca(OH)$_2$ dissolution without CaCO$_3$ precipitation, second, assuming as much CaCO$_3$ precipitation as the amount of TA added, third, assuming CaCO$_3$ precipitation happening until reaching an Ω_A of 2, and fourth, CO$_2$ uptake until equilibrium is reached between atmosphere and seawater at a pCO$_2$ of ~416 µatm.
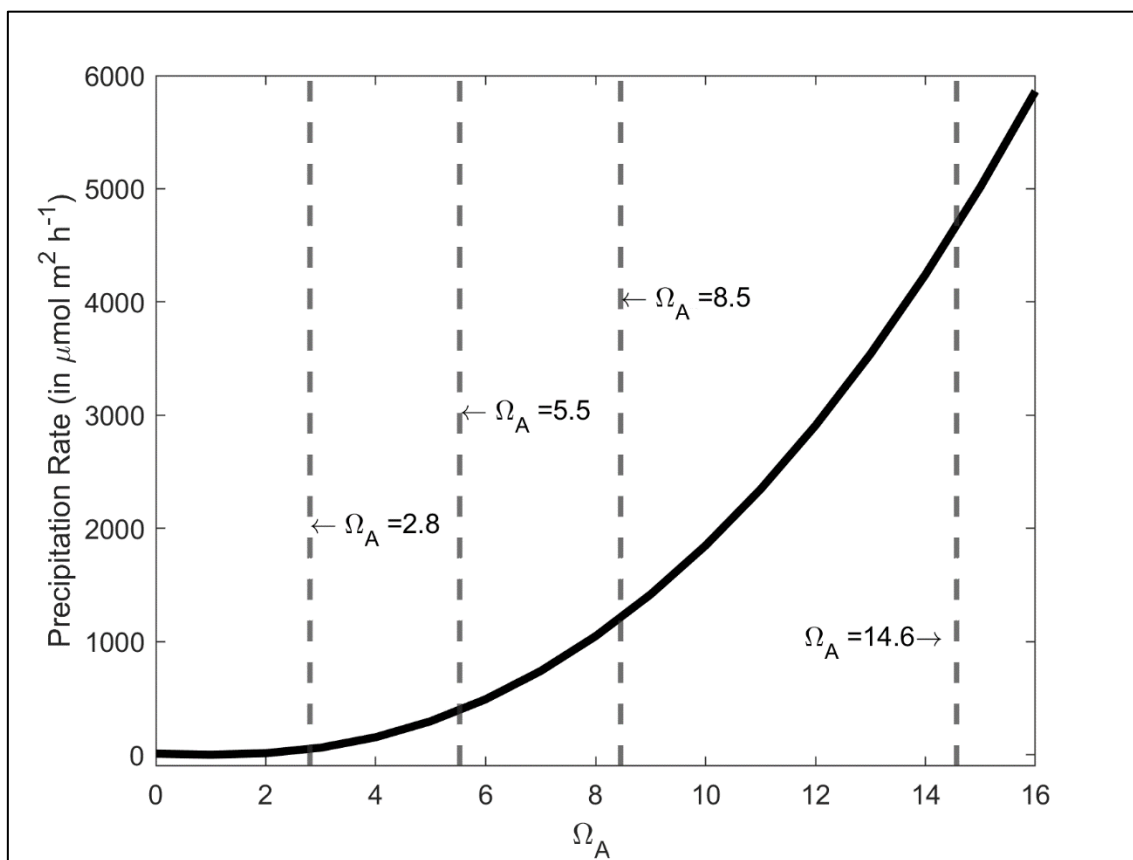
735 **Figure A4: CaCO₃ precipitation rate onto aragonite seed crystals in μmol m⁻² h⁻¹ as a function of Ω_A, based on the measurements of Zhong and Mucci (1989) at 25 °C and for a salinity of 35. The Ω_A values for the starting conditions, and following a +250, +500 and +1000 μmol kg-1 TA increase are presented by the grey dashed lines, i.e., 2.8, 5.5, 8.5 and 14.6 respectively.**
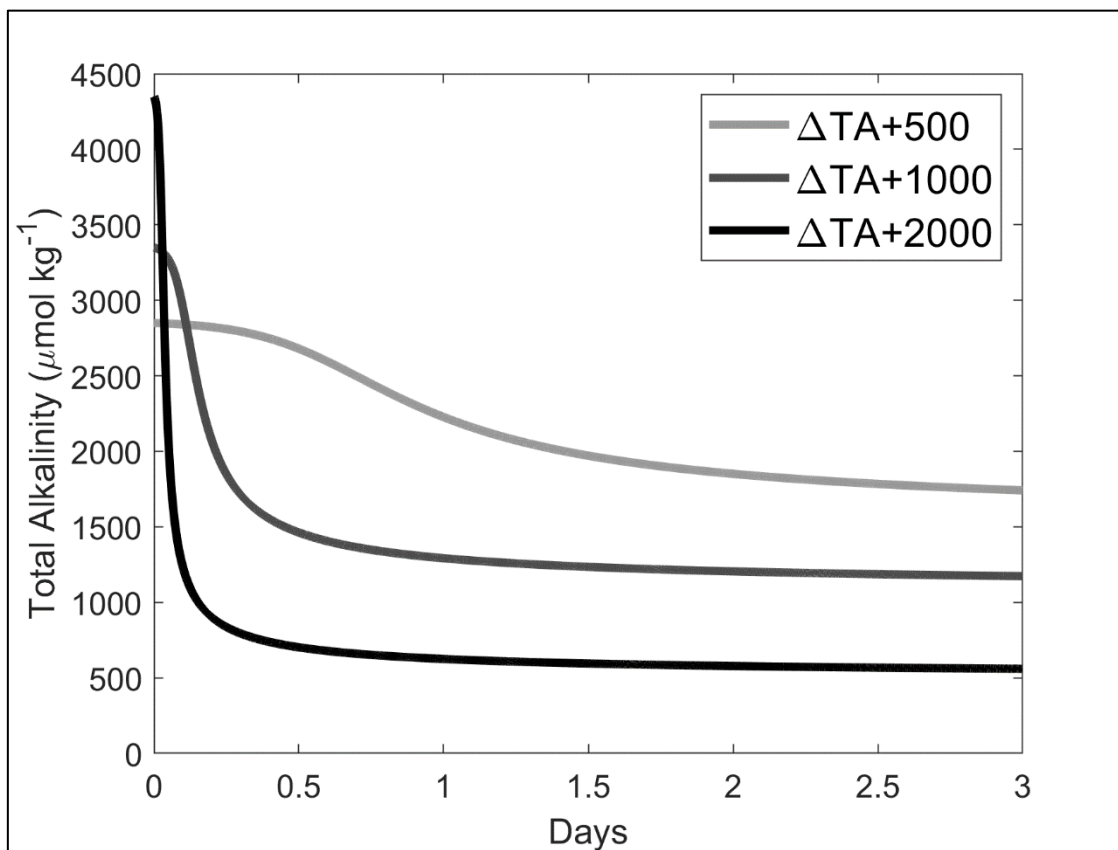
740 **Figure A5: Simulations of TA loss due to aragonite precipitation after a TA addition of 500, 1000 and 2000 μmol kg⁻¹, based on Ω_A and surface area dependant precipitation rates shown in Figure A4, assuming the initial presence of 2% of CaCO₃ in our samples, i.e., ~0.37, ~0.74 and ~1.48 mg kg⁻¹ for a ΔTA+500, ΔTA+1000 and ΔTA+2000 μmol kg⁻¹, respectively. CaCO₃ mass was converted to a surface area as described in Zhong and Mucci (1989). The starting conditioned were TA = 2300 μmol kg⁻¹, DIC = 2100 μmol kg⁻¹, salinity = 35 and temperature = 21 °C.**